Chapter 6 | Dark Matter in Spiral Galaxies

ABSTRACT– This chapter discusses the shapes of galaxy rotation curves and the structural properties of dark matter haloes in which spiral galaxies seem to be embedded. A comparison is made between observed HI rotation curves and the so-called 'universal' rotation curve. We find that for about one third of the observed rotation curves the shapes deviate significantly from this 'universal' rotation curve shape. We derived structural parameters of dark matter haloes for both isothermal sphere and Hernquist models. Various fits with different assumptions about the stellar mass-to-light ratios were made. Maximum-disk, sub-maximum-disk, equal-(M/L) and constrained-halo decompositions were performed. We conclude that the inferred structural properties of the dark matter haloes strongly depend on the adopted stellar mass-to-light ratios. In the case of maximum-disk fits we find for the high surface brightness galaxies that the near-infrared stellar mass-to-light ratios lie in the range 0.4-1.0 and do not vary with color or morphological type. There are at most marginal trends between the structural parameters of the haloes and the amounts and distributions of the luminous mass. There is some evidence for a kinematic signature of the bimodality of surface brightness distribution discussed in Chapter 3. Finally, a comparison is made between the rotation curves of three galaxies of the same luminosity but with different distributions of the stellar component. The decomposition of their rotation curves showed that the same halo can be adopted for all three systems while only minor differences in the K' mass-to-light ratios are required to obtain satisfactory fits to the observed rotation curves. This result supports the idea that galaxies of the same luminosity live in similar haloes regardless of the distribution of their luminous mass.

1 Introduction

Information about the present-day distribution of dark matter in and around galaxies should lead to a better understanding of the conditions and processes which initiated and guided the formation of galaxies out of the initial density perturbations in the early universe. The density and extent of a dark matter halo is for instance closely related to the epoch of its formation and the density of the universe at the time the halo started to collapse. An early collapse in a young, high density universe will result in a small compact halo, while haloes that collapse at a later stage will be larger and more diffuse. Consequently, in the framework of hierarchical clustering, one would expect that present-day dwarf galaxies live in more compact, denser haloes than the more massive systems. Moreover, the detailed radial behaviour of the density of dark matter within a collapsed halo is related to the slope of the power spectrum of the initial density perturbations. Two kinds of density profiles for a dark matter halo are now widely accepted as plausible outcomes of the process of galaxy formation. One is the density profile which corresponds to an isothermal sphere of dark matter and the other is the so-called Hernquist (1990) density profile. The former one can be justified on theoretical grounds (e.g. Hoffman, 1988) while the latter density profile has emerged empirically from numerical simulations (e.g. Dubinski and Carlberg 1991, Navarro *et al*, 1996 and 1997).

This chapter deals only with the observational aspects related to these issues, and presents a discussion

Table 1: Photometric and kinematic information for the 30 members of the Ursa Major Cluster sample with relatively unperturbed HI kinematics.

nr.	Name	Type	i	$M_T^{b,i}(B)$	$M_T^{b,i}(K')$	$\mu_0^i(K')$	$r_d(K')$	C_{82}	$R_{25}^{b,i}(B)$	$R_{80}(I)$	R^{lmp}	V_{max}	V_{flat}
			(°)	(mag)	(mag)	(mag/$''^2$)	(kpc)		(′)	(′)	(′)	(km/s)	(km/s)
(1)	(2)	(3)	(4)	(5)	(6)	(7)	(8)	(9)	(10)	(11)	(12)	(13)	(14)
1	U6399	Sm	75	-17.76	-19.93	19.28	1.98	3.3	0.91	1.08	1.50	88	88
2	U6446	Sd	51	-18.03	-19.48	19.84	1.49	4.1	1.02	1.33	2.93	82	82
3	N3726	SBc	53	-20.58	-23.02	17.72	2.84	3.1	2.63	2.01	6.22	162	162
4	N3729	SBab	49	-19.22	-22.38	16.86	1.40	3.5	1.29	1.07	1.00	151	151
5	U6667	Scd	89	-18.04	-20.25	20.44	2.43	3.3	1.08	1.59	1.50	86	86
6	N3877	Sc	76	-20.24	-23.28	17.12	2.34	3.2	1.95	1.74	2.17	167	167
7	U6773	Sm	58	-17.22	-19.76	19.48	1.26	3.3	0.67	0.66	0.67	45	...
8	N3917	Scd	79	-19.65	-21.97	18.66	2.57	3.0	1.72	1.65	2.83	135	135
9	N3949	Sbc	55	-20.07	-22.56	17.08	1.44	3.7	1.31	0.81	1.35	164	164
10	N3953	SBbc	62	-20.68	-23.96	17.22	3.20	4.4	2.63	2.03	3.00	223	223
11	U6894	Scd	83	-17.10	-18.66	20.35	1.26	3.1	0.56	0.66	0.67	63	...
12	N3972	Sbc	77	-19.10	-21.64	17.90	1.62	3.0	1.29	1.24	1.67	134	...
13	U6917	SBd	56	-18.49	-20.69	19.83	2.43	3.4	1.40	1.47	2.00	104	104
14	N3985	Sm	51	-18.35	-20.79	17.56	0.95	2.9	0.64	0.46	0.50	93	...
15	U6923	Sdm	65	-17.86	-19.95	18.80	1.08	5.0	0.82	1.09	1.02	81	...
16	N3992	SBbc	56	-20.75	-23.75	17.45	3.47	4.0	3.05	2.39	6.67	272	242
17	N4013	Sb	90	-19.93	-23.38	16.44	1.71	3.7	1.78	1.71	6.12	195	177
18	N4010	SBd	89	-19.01	-21.84	19.41	2.89	2.9	1.46	1.81	2.00	128	128
19	U6969	Sm	76	-17.02	-18.45	20.34	1.13	3.0	0.58	0.60	0.85	79	...
20	U6983	SBcd	49	-18.44	-20.46	19.87	2.21	3.8	1.46	1.40	3.00	107	107
21	N4085	Sc	82	-19.29	-21.86	17.36	1.31	3.2	1.03	0.90	1.18	134	134
22	U7089	Sdm	80	-18.64	-19.95	20.53	2.57	3.5	1.22	1.58	1.75	79	...
23	N4100	Sbc	73	-20.14	-23.00	17.11	2.12	2.9	2.01	1.53	4.35	195	164
24	U7094	Sdm	70	-17.16	-19.42	19.68	1.22	4.5	0.64	0.98	1.00	35	...
25	N4102	SBab	56	-19.58	-23.12	16.78	1.49	7.6	1.33	0.87	0.83	178	178
26	N4138	Sa	53	-19.30	-22.79	16.48	1.17	5.3	1.10	0.75	3.55	195	147
27	N4157	Sb	82	-20.27	-23.54	16.77	2.16	3.9	2.30	2.07	5.67	201	185
28	N4183	Scd	82	-19.41	-21.30	19.47	2.66	3.2	1.55	1.86	4.02	115	109
29	N4218	Sm	53	-17.88	-20.15	17.06	0.54	3.2	0.53	0.34	0.33	73	...
30	N4217	Sb	86	-20.22	-23.45	17.17	2.43	3.3	2.11	2.12	3.17	191	178

of the structural parameters of the dark matter haloes as inferred from observed rotation curves of spiral galaxies. Both the isothermal sphere and the Hernquist profiles will be considered when decomposing the rotation curves into the main dynamical constituents of a spiral galaxy, i.e. a gaseous disk component, the stellar component and the dark matter halo.

Here the observed rotation curves are analysed in the framework of Newtonian gravity. It should be noted, however, that the concept of modified Newtonian dynamics (Milgrom, 1983) is very succesful in relating the shapes of observed rotation curves directly to the luminous mass in galaxies (e.g. Sanders and Begeman 1994, Begeman *et al* 1991).

For our study we selected a complete, volume limited sample of spiral galaxies in the nearby Ursa Major Cluster (Tully *et al* 1996: Chapter 2). These galaxies cover a wide range of luminosities, morphologies and surface brightnesses. For each galaxy we obtained optical and near-infrared surface photometry to determine the distribution of the stellar component and 21cm-line line observations to derive the HI density distribution and the rotation curve.

We briefly describe the sample and the observations in Section 2 and the shapes of the rotation curves in Section 3. In Section 4 we describe the density profiles of the isothermal sphere and the Hernquist halo. The performed decompositions are explained in Section 5 and the results are presented in Section 6. In Section 7 we investigate a possible kinematic signature of the bimodality of surface brightnesses as described in Chapter 3. In Section 8 we compare the shapes and decompositions of the rotation curves of three galaxies with the same luminosity but different surface brightness distributions. Finally, Section 9 presents the conclusions.

2 The sample

The galaxies we consider here are from the Ursa Major cluster sample described in Chapter 2. Since all these galaxies are nearly at the same distance, there is little doubt about their relative luminosities, masses and sizes. There are 49 galaxies intrinsically brighter than the SMC and more inclined than 45 degrees of which 30 systems show relatively unperturbed HI kinematics. The other 19 systems are HI poor S0s, are involved in serious interactions or show global non-circular motions. The optical and near-infrared photometry of these 30 spirals is presented in Chapter 2. The HI synthesis observations from which the rotation curves and the radial HI surface density profiles were obtained are presented in Chapter 4.

Table 1 gives a summary of the global properties of these galaxies.
Column (1) contains a number for references in subsequent figures.
Column (2) gives the NGC or UGC number.
Column (3) provides the morphological type and
Column (4) the inclination angle.
Columns (5-6) give the corrected total absolute magnitudes in the B and K' passbands.
Column (7) contains the near-infrared face-on disk central surface brightness and
Column (8) gives the disk scale length as derived from the K' luminosity profile.
Column (9) provides the compactness parameter which is defined as $C_{82} \equiv R_{80}/R_{20}$, the ratio of the radii which enclose 80% and 20% of the total light. For an exponential disk C_{82} is independent of scale length but will increase with increasing bulge-to-disk ratio.
Columns (10-12) provide the radius of the corrected 25^{th} B-mag/$''^2$ isophote, the radius which encloses 80% of the I-band light and the radius of the last measured point on the rotation curve.
Column (13) gives the maximum rotational velocity and
Column (14) provides the amplitude of the outer flat part of the rotation curve which is occasionally lower than V_{max}. In some cases the HI disk is not extended enough to reach the flat part of the rotation curve.

3 The shapes of rotation curves

The shapes and amplitudes of rotation curves of spiral galaxies are directly related to the gravitational potential in the plane of the disk which arises from the combined distribution of luminous and dark matter. If the luminous mass embedded in the dark halo is of any dynamical importance, the shapes of rotation curves are expected to differ among galaxies of the same luminosity but with different luminosity profiles. The presence of a dark matter halo will moderate these differences and, if the dark matter halo is dynamically dominant, the shapes of rotation curves will largely be independent of the light distribution. In this section we will investigate the shapes of the rotation curves as a function of the distribution of the luminous mass.

Results from the first measurements of galaxy rotation curves have led to the generic picture that rotation curves show a steep rise in the inner regions, after which they turn over and remain flat to the last measured point, often well beyond the radius of a detectable stellar disk (van Albada and Sancisi 1986, Casertano and van Albada, 1990). Clearly, such a shape of the rotation curve deviates from what one would expect given the exponential distribution of light in a spiral galaxy (Freeman, 1970). Although the shape of the rotation curve in the inner regions can be reconciled with the distribution of luminous mass (Kalnajs 1983, Kent 1986), the extended flat part can only be explained by introducing an additional dynamical component, the dark matter halo. The radial density profile of a dark matter halo seems to compensate for the decreasing contribution of the luminous matter to the gravitational potential beyond about 2 scale lengths in such a way that the rotation curve remains nearly flat. This effect is known as the 'disk-halo conspiracy' (van Albada and Sancisi 1986).

This generic picture of the flat shapes of rotation curves has been progressively refined since the mid-seventies, using optical and HI rotation curves. Optical rotation curves typically do not extend much beyond two-thirds of R_{25} and map the kinematics in the inner regions of galaxies only. The more extended HI rotation curves are necessary to study the shapes of rotation curves in the outer regions of spiral galaxies. In this respect, optical and HI rotation curves should be considered complementary to each other.

Using optical rotation curves of Sa-Sc spirals, Rubin *et al* (1985) noted that the shape of the rotation curves in the inner regions are not related to the morphological type of a galaxy. The steepness of rotation curves in the inner regions are more related to the luminosity of a spiral than to its morphology. From this they concluded that dark matter must be the dynamically dominant component at all radii, even in the very centers of spirals.

On the other hand, some rotation curves show detailed features in the inner regions which can be related to corresponding features in the luminosity profiles (e.g. Kent, 1986). This notion gave support to the maximum-disk hypothesis, which postulates that the luminous matter is the dominant dynamical component in the central regions of galaxies (van Albada and Sancisi 1986). This hypothesis was put forward to derive lower limits on the amounts of dark matter in spirals.

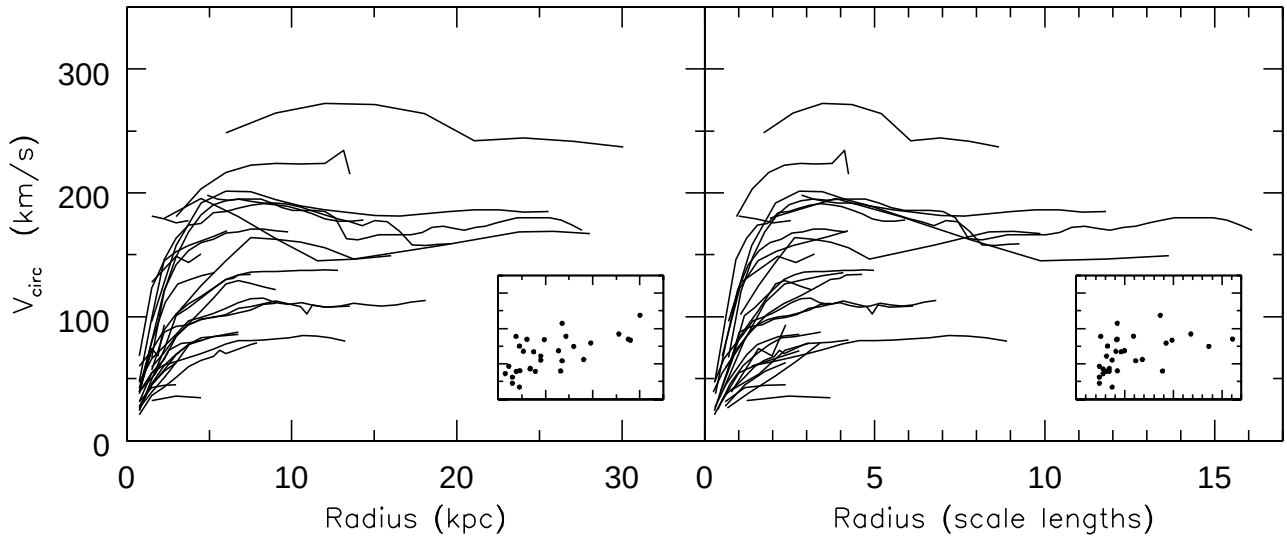

Figure 1: Compilation of rotation curves of all kinematically unperturbed spirals in the Ursa Major Cluster plotted on the same linear scale (left panel) and scaled with the disk scale length (right panel). The insets show the positions of the last measured points.

Casertano and Van Gorkom (1991) investigated the shapes of the rotation curves in the outer regions of galaxies using HI synthesis data. They found that rotation curves are not always simply flat after they turn over but can show a significant decline in their outer regions, sometimes until their last measured point. Such a decline occurs mainly in galaxies with short photometric scale lengths and in the most massive systems. In those galaxies, the luminous mass is concentrated to such a degree that its contribution to the local potential dominates over that of the dark halo. In such cases the disk-halo conspiracy apparently breaks down to a certain extent.

Figure 1 shows the rotation curves of the 30 spiral galaxies in the Ursa Major cluster with kinematically unperturbed gas disks (see Chapters 4 and 5). In the left panel the rotation curves are plotted on the same linear scale. Since all galaxies are nearly at the same distance, there is little doubt about the relative extent of their rotation curves in terms of kiloparsec. In the right hand panel the rotation curves are scaled with the scale length of the exponential disk in the K'–band. The rotation curve from a purely exponential disk reaches its maximum rotational velocity at 2.2 disk scale lengths. Note that several rotation curves are still rising at that radius. This may indicate for instance that the gas component or the dark matter halo are already dynamically important at that radius or that the luminosity profiles are shallower than exponential.

The positions of the last measured points of the rotation curves in each panel are plotted separately in the insets. They show that in general the rotation curves of more massive galaxies can be measured at larger radii, in terms of kiloparsec, than those in less massive systems. In terms of scale lengths this is less the case. Therefore, care should be taken when comparing mass-to-light ratios within a fixed number of scale lengths or within the radius of the last measured point as a function of luminosity or V_{max} since the inferred total mass enclosed by a particular orbit depends on the radius of that orbit in kiloparsec.

Figure 2 shows the rotation curves as a function of global morphology. Although the few Sa galaxies in our sample have rotational velocities comparable to those of the Sb systems, the well known correlation between morphology and rotational velocity is evident. The Sa systems reach their maximum rotational velocity closer to the center than Sb galaxies with similar asymptotic velocities. Furthermore, we find a wide range of rotational velocities among the Sb-Sc galaxies, varying between 80 and 250 km/s. Finally, note that there are four Sb galaxies (NGC 4013, 4100, 4157 and 4217) with nearly identical rotation curves which show a slight decline between 8 and 15 kpc. These four spirals also have very similar luminosities ($-23.49 < M_{K'} < -22.98$), exponential disk scale lengths ($1.7 < r_{d\,(\mathrm{kpc})} < 2.4$) and central disk surface brightnesses ($16.44 < \mu_0^i(K') < 17.17$).

In general, the morphological classification of a spiral is closely related to the overall distribution of the light and can be quite subjective. If the shapes of rotation curves in the central regions of galaxies are related to the distribution of the luminous matter, one would expect to see differences between galaxies with a purely exponential disk and galaxies with a more centrally concentrated distribution of light, regardless of

their morphology.

In Figure 3, the rotation curves are plotted according to a more quantified assessment of the distribution of the stellar light. In the left six panels the rotation curves are plotted in kiloparsec, and in the right six panels they are scaled with the disk scale length. The upper panels make a distinction between high surface brightness (HSB) and low surface brightness (LSB) galaxies. The distinction between HSB and LSB galaxies is made in the spirit of Chapter 3. In case the face-on (extrapolated) central disk surface brightness in the K'–band $\mu_0^i{}_{(K')}$ is fainter than 18.5 mag/arcsec^2, a galaxy is considered to be LSB and if $\mu_0^i{}_{(K')}$<18.5 mag/arcsec^2 it is HSB. The maximum observed rotational velocities of LSB galaxies in our sample do not exceed ≈150 km/s. The most massive, barely LSB system is NGC 3917 with $\mu_0^i{}_{(K')}$=18.66 mag/arcsec^2 and V_{max} = 135 km/s. The faintest HSB system is NGC 4218, but the rotation curve of this blue compact dwarf is only marginally resolved and is apparently still rising at the last measured point. We do not find declining rotation curves in our LSB galaxies.

In the lower panels of Figure 3, the rotation curves are grouped according to the disk scale length r_d and the compactness $C_{82}\equiv R_{80}/R_{20}$ of the luminous matter. Note that the compactness parameter is related to the relative importance of a bulge component or any central concentration of the light. For a purely exponential disk C_{82}=3.63 and is independent of scale length. The limits on C_{82} and r_d were chosen empirically in such a way that the rotation curves are distributed more or less evenly over the four panels. Declining rotation curves are mainly found in galaxies with a more compact (C_{82}>3.2) distribution of the light. The three Sa-Sab galaxies in our sample are compact and have small scale lengths. They can be found in the upper left of each block of four adjacent panels. There does not seem to be a significant correlation between the shape of the rotation curve and the scale length of the disk.

Casertano and Van Gorkom (1991), however, noted that the shapes of rotation curves do depend on the scale length r_d of the exponential disk and the maximum rotational velocity V_{max} of a galaxy. Figure 4 shows our rotation curves in a V_{max}–r_d plot in which the curves are plotted in a similar fashion as those by Casertano and Van Gorkom. The origin of each rotation curve indicates the scale length of the exponential disk in kpc and the maximum rotational velocity. Each rotation curve is scaled individually both in radius and in amplitude. In the radial direction each curve is scaled by $20r_d$ so, in terms of scale lengths, each rotation curve extends twenty times further from the origin than the scale of the abscissa suggests. The horizontal bar at each origin indicates 1 scale length. The rotation curves are also scaled in amplitude and the vertical bar at the origin indicates 20 km/s. The labels refer to the entry numbers in Table 1. Our rotation curves populate only a limited

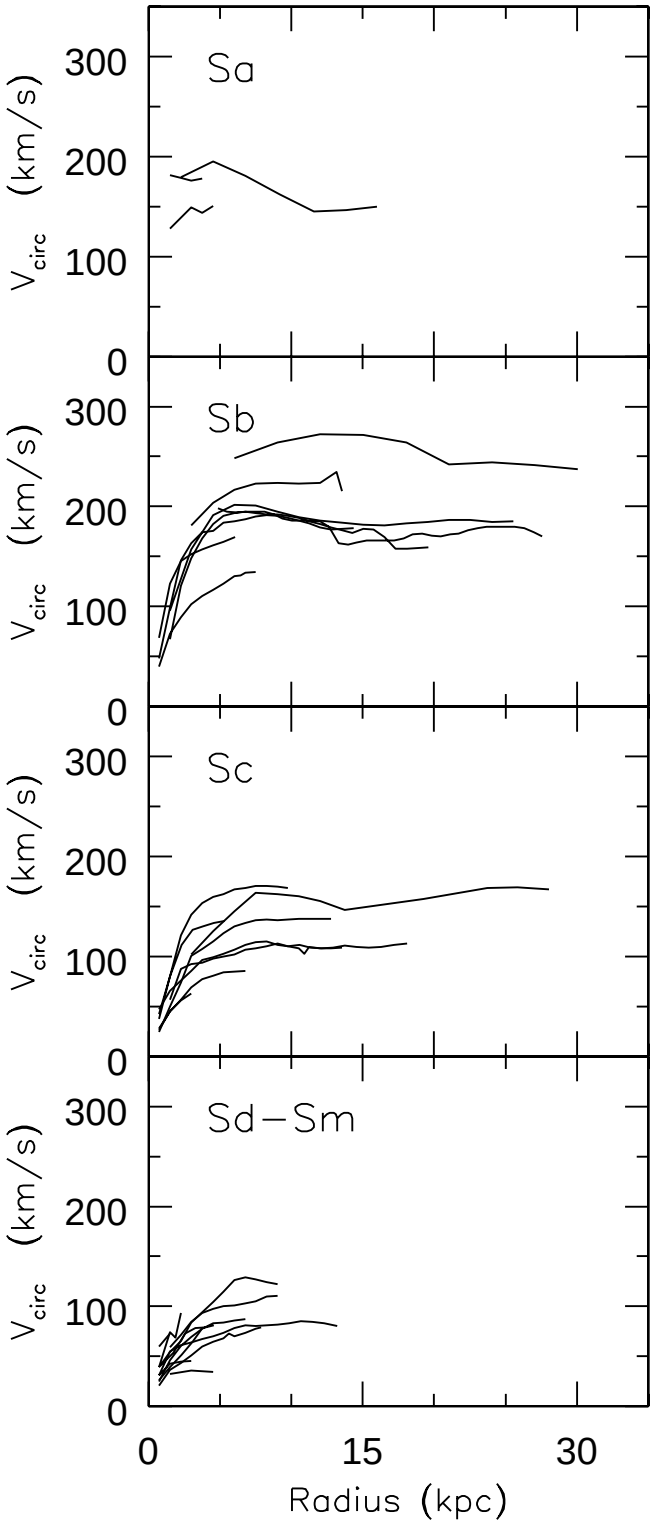

Figure 2: The shapes of the rotation curves as a function of morphological type.

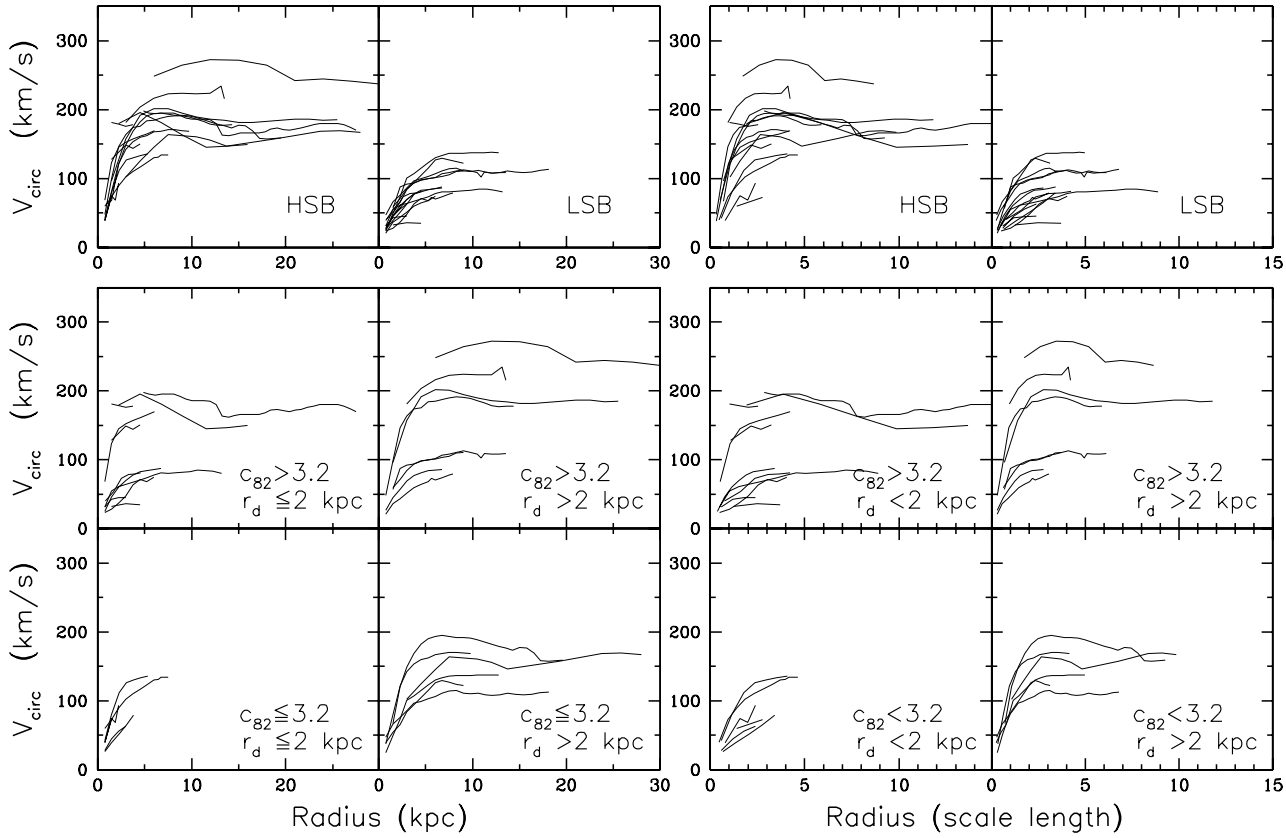

Figure 3: The shapes of the rotation curves as a function of the distribution of the luminous mass, plotted in kiloparsecs and in disk scale lengths. The upper panels make a distinction between high and low surface brightness galaxies. The lower panels make a distinction between galaxies with small and large scale lengths (r_d<2 kpc<r_d) and with or without a central concentration (C_{82}<3.2<C_{82} with $C_{82}\equiv R_{80}/R_{20}$).

area of the V_{max}–r_d parameter space covered by Casertano and Van Gorkom and therefore, the correlation between the shapes of our rotation curves and the values of V_{max} and r_d are only marginal. Casertano and Van Gorkom noted that declining rotation curves are mainly found in the upper left part of the diagram while rising rotation curves are found among the dwarf galaxies in the lower part of the figure. They devised 4 classes of galaxies:

Large bright	: V_{max}>180 km/s, r_d>3.5 kpc.
Compact bright	: V_{max}>180 km/s, r_d<3.5 kpc.
Intermediate	: 100<V_{max}<180 km/s.
Dwarf	: V_{max}<100 km/s.

Note that they use the word 'compact' for galaxies with short scale lengths. Their concept of compactness is unrelated to our compactness parameter C_{82}. In Figure 5, our rotation curves are displayed in the panels that correspond to each of the classes which are identified in Figure 4. All galaxies with a declining rotation curve in our sample belong to the class of compact bright systems. Note that our sample of unperturbed rotation curves lacks large bright spiral galaxies. Due to this lack of large bright systems, we can not confirm nor falsify the claim by Casertano and Van Gorkom that bright galaxies with declining rotation curves have small scale lengths while bright galaxies with large scale lengths have flat rotation curves. The one galaxy in our sample which just falls outside the class of large bright systems is NGC 3992 and this galaxy does have a declining rotation curve. The largest galaxy in the Ursa Major cluster, NGC 3718, would have been classified as a large bright system but this galaxy is severly perturbed and its rotation curve is ill defined. Nearly all the dwarf galaxies in our sample have rotation curves which are still rising at the last measured point while the rotation curves of the intermediate galaxies do show the generic flattened shape. In this respect, our sample of rotation curves does follow the trend outlined by Cassertano and Van Gorkom. The dependency of the rotation curve shape with scale length among the bright systems, which we can not address with our data, was discussed by Broeils (1992) with a sample of 23 spirals. He finds that most of the 8 large bright

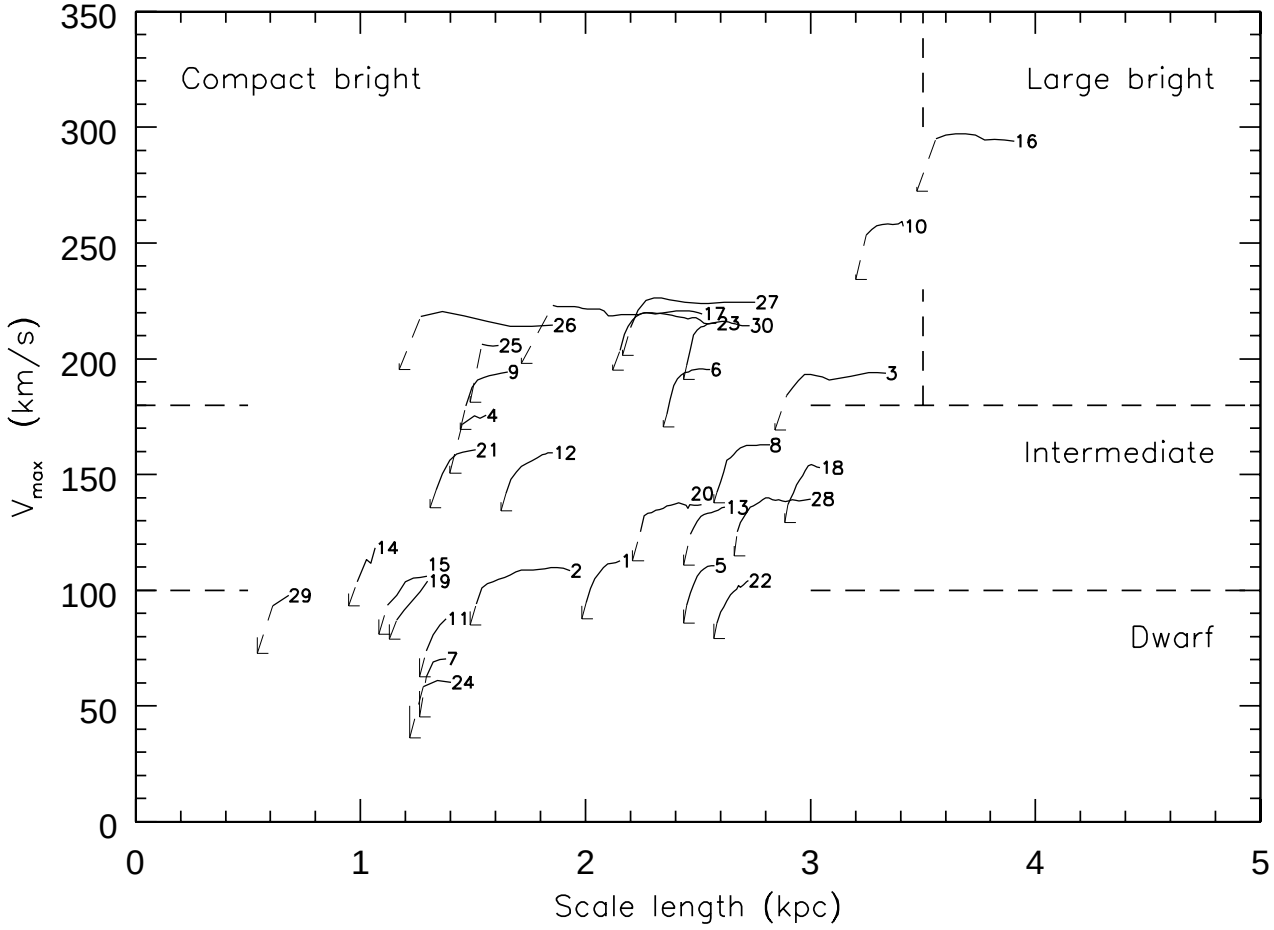

Figure 4: Compilation of rotation curves following Casertano and Van Gorkom (1991). The origin of each curve corresponds to the scale length of the stellar disk and the maximum rotational velocity in the rotation curve. To avoid confusion, all rotation curves are scaled in radius and velocity.

spirals in his sample do show declining rotation curves, contradicting the claim by Casertano and Van Gorkom.

the 'universal' rotation curve

From numerical simulations of the formation of dark matter haloes the concept of a universal rotation curve (URC) has emerged (Navarro *et al* 1997) and it has become of prime interest to relate the observed shapes of rotation curves to the results from these simulations (e.g. Persic *et al*, 1996, Hernandez and Gilmore, 1997). It is claimed by Persic and Salucci (1991) that the *observed* rotation curves of galaxies also follow a universal shape, solely as a function of luminosity. Persic *et al* (1996) established this universal shape by averaging observed rotation curves in eleven luminosity bins using a sample of 714 optical rotation curves from Mathewson *et al* (1992) supplemented by 33 HI rotation curves. They provide the following functional form:

$$V_{URC}(x) = V(R_{opt})\left[(0.72+0.44log\lambda)\frac{1.97x^{1.22}}{(x^2+0.78^2)^{1.43}}+1.6e^{-0.4\lambda}\frac{x^2}{x^2+2.25\lambda^{0.4}}\right]^{\frac{1}{2}}$$

where λ=L/L$_*$ with log(L$_*$/L$_\odot$)=10.4 in the *B*-band and x=R/R$_{opt}$ with R$_{opt}$ the radius which encloses 83% of the light. For an exponential disk with scale length r$_d$, R$_{opt}$ = 3.2r$_d$. V(R$_{opt}$) is the rotational velocity at the radius R$_{opt}$ given by

$$V(R_{opt}) = \frac{200\lambda^{0.41}}{\left[0.80+0.49log\lambda+\frac{0.75e^{-0.4\lambda}}{0.47+2.25\lambda^{0.4}}\right]^{\frac{1}{2}}}$$

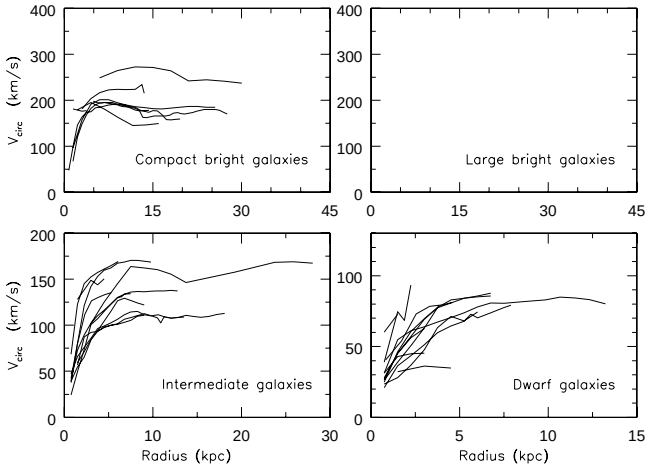

Figure 5: The shapes of the rotation curves as classified according to Casertano and Van Gorkom (1991).

With this prescription, the shape of the rotation curve does not depend on the actual distribution of the light within the dark matter halo. However, the value of R_{opt} is relatively smaller for galaxies with a bulge component than for galaxies without a bulge. Consequently, an observed rotation curve which is scaled by R_{opt} will become shallower if a bulge component is present, and hence will more resemble a rotation curve of a bulge-less galaxy of the same luminosity.

The optical rotation curves used by Persic *et al* were derived for Sb-Sd galaxies and because Sa galaxies in general do not show extended HI disks, Persic *et al* make a disclaimer about the validity of the URC for early type spirals with a considerable bulge component. Below, we will consider our observed HI rotation curves of spirals in the Ursa Major Cluster and investigate whether their shapes follow this universal rotation curve.

In Figure 6 we split our sample into 4 luminosity bins to avoid too much confusion. In the left column the rotation curves are plotted on the same linear scale in each panel, in the middle column they are scaled with R_{80} and in the right column they are radially scaled with the scale length of the exponential disk. For galaxies with a considerable bulge component, R_{80} may be relatively much smaller than $3.2r_d$ compared to galaxies without a bulge. In the middle and right columns the URC is plotted for various luminosities. We make the approximation that $R_{opt} \equiv R_{83} \approx R_{80}$ since we did not measure R_{opt} for our galaxies. The URCs in the right column are plotted under the assumption of purely exponential disks for which $R_{opt}=3.2r_d$. Consistent comparisons between our rotation curves and the URC should be made in the panels of the middle column. At first glance, our observed rotation curves follow the URC pretty well especially in the inner parts. However, in nearly every luminosity bin we can identify rotation curves that rise too steeply in the inner regions or which show a declining rotation curve inconsistent with the URC for that luminosity class.

These deviating galaxies are grouped together in a single panel in Figure 7. In the upper panels, the rotation curves which more or less follow the URC are plotted and in the lower panels we have plotted the ten rotation curves which clearly deviate from the 'universal' shape. Some rotation curves deviate significantly from the shape described by the URC. Among the fainter galaxies we find rotation curves that rise steeper than the URC, while several galaxies with rotational velocities between 150 and 200 km/s show a decline in their outer regions, not accommodated by the URC prescription. The galaxies in which these deviating curves were measured are N3729, N4013, N4100, N4102, N4138, N4157, N4183, N4217, U6446 and U6983. The median value of the scale length for these 10 galaxies is similar to that of the entire sample (1.9 vs 2.0) while the median value of C_{82} is slightly larger than that of all 30 galaxies (3.8 vs 3.2).

Note that the URC found by Navarro *et al* is related to the dark matter halo. The observationally established URC comprises contributions from all dynamically important constituents of a spiral galaxy, not just the halo. Therefore, an elaborate transformation scheme is worked out by Persic *et al* to allow a proper comparison between the observational and numerical URC.

4 Mass models for dark haloes

Although the shape of rotation curves in the inner regions of galaxies can largely be explained by the distribution of the luminous mass, the constant rotational velocity in the extended outer parts cannot. Assuming Newtonian gravity from the luminous mass, rotation curves are expected to drop in the outer regions. However, the observational fact that they remain more or less flat can only be understood by introducing an additional, unseen component, the dark matter. It is a priori unclear what the 3-dimensional density distribution of this matter is. Although much research is aimed at improving our understanding of the 3-dimensional geometry using a variety of methods (e.g. using e.g. the thickness of the HI disk; Olling 1996, Sicking 1997; non-circular motions; Franx and de Zeeuw 1992; anisotropic velocity dispersions of satellite galaxies; Zaritsky *et al* 1997) there is still no convincing solid result which unambiguously excludes a simple spherical distribution. Therefore, the most simple geometry, a sphere, is adopted here. Because the observed rotation curves are nearly flat in the outer parts, the density within this spherical distribution should decrease with radius like $1/r^2$ in the region where the rotation curves

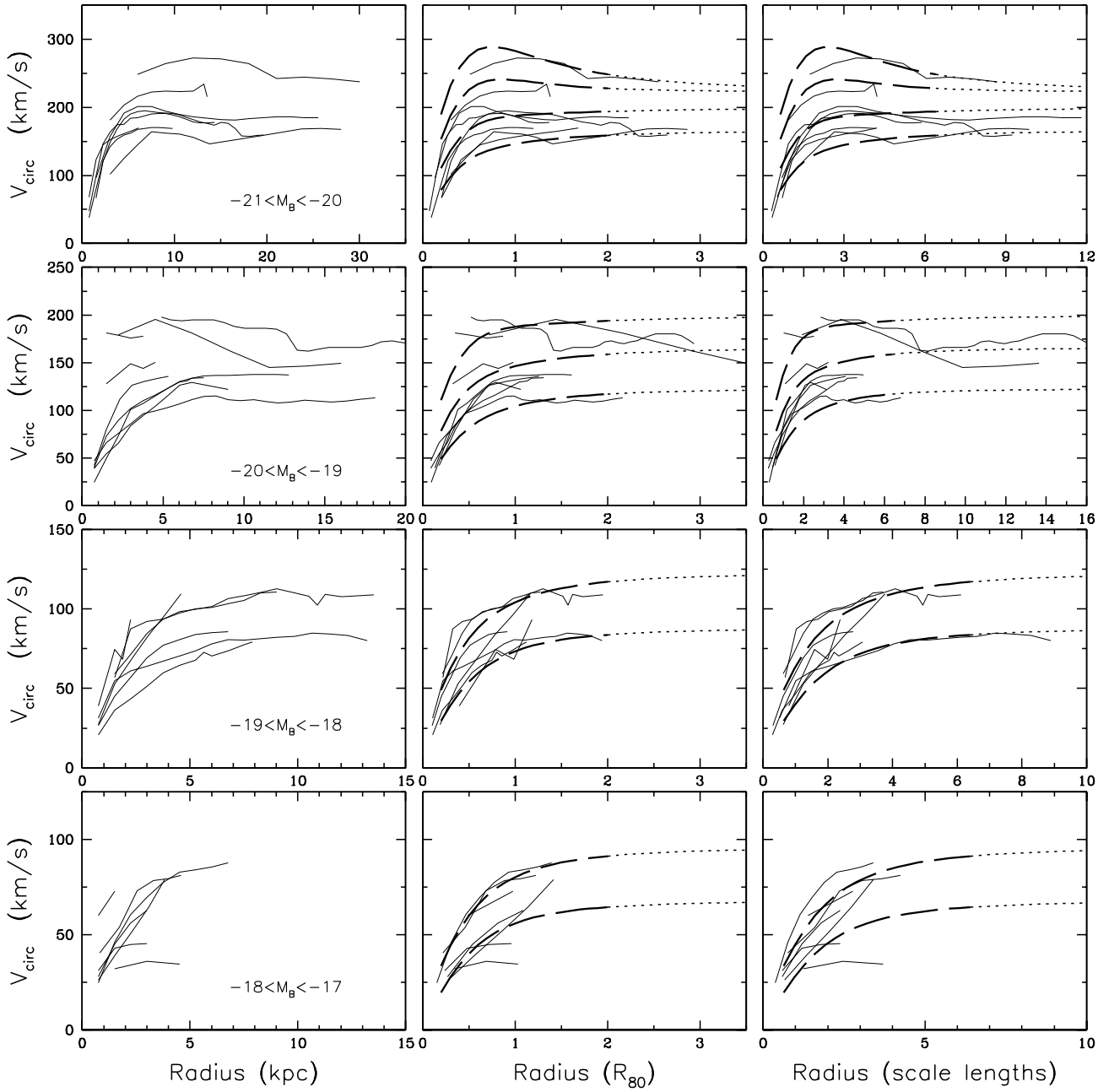

Figure 6: A comparison between the shapes of rotation curves and the universal rotation curve as proposed by Persic *et al* (1996). To avoid too much confusion the rotation curves are plotted in four luminosity bins. In the left column the rotation curves are plotted in kiloparsec. In the middle column the rotation curves are scaled radially with R_{80} which is effectively the scaling factor applied by Persic *et al*. In the right column, the rotation curves are scaled radially by the disk scale length. The dashed/dotted cuves indicate the shape of the 'universal rotation curve' which is roughly defined until $2R_{80}$. For the URCs plotted in the right column it is assumed that $R_{80}=3.2r_d$.

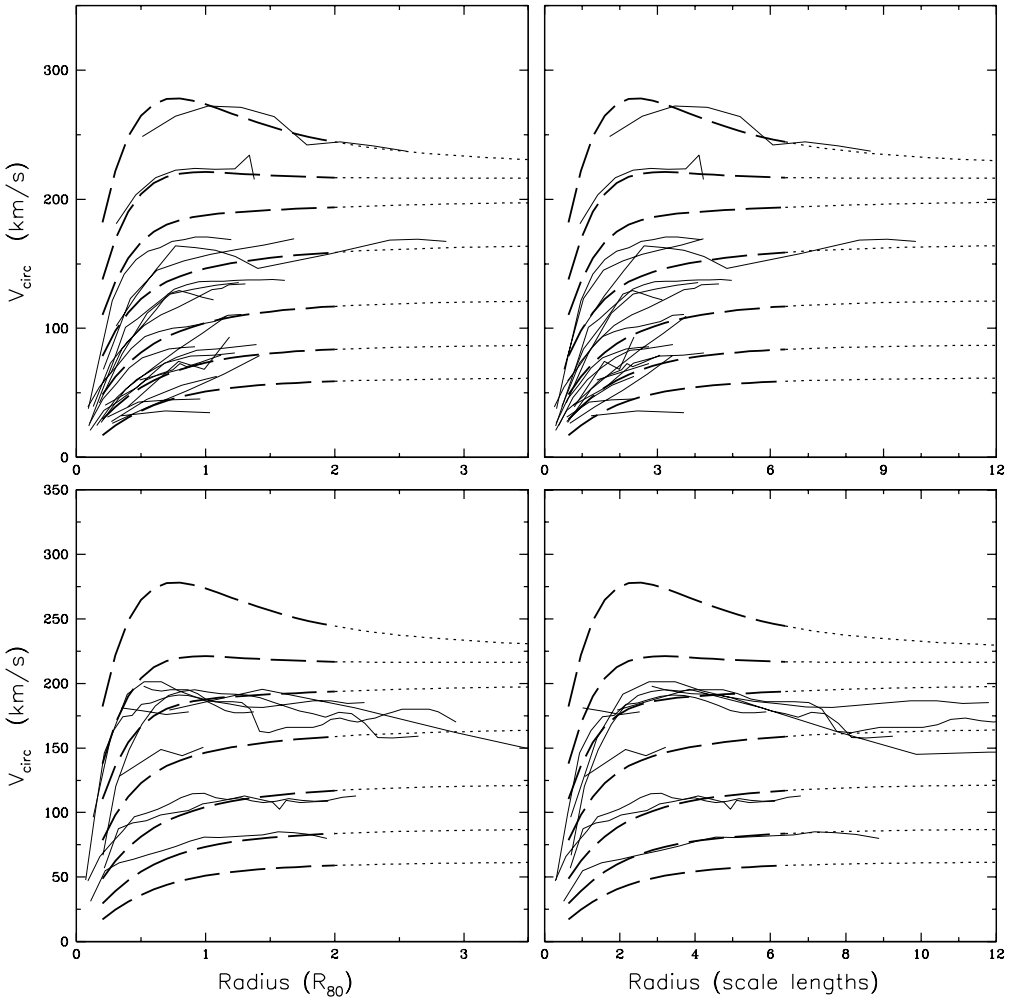

Figure 7: A comparison between the observed shapes of rotation curves and the 'universal' rotation curve. The observed rotation curves in the upper panels are in reasonable agreement with the URC shape. The lower panels, however, show that some rotation curves deviate significantly from the URC shape.

are observed. Here we will consider the isothermal sphere with a core of constant density and the Hernquist model for the radial density profiles.

a) The isothermal sphere

The radial density profile of an isothermal sphere with a core of radius R_c and a constant central density ρ_0 is given by

$$\rho(R) = \rho_0 \left[1 + \left(\frac{R}{R_c}\right)^2\right]^{-1}$$

This spherically symmetric radial density profile gives rise to a halo rotation curve of the form

$$V_{\rm halo}^2(R) = 4\pi G\rho_0 R_c^2 \left[1 - \frac{R_c}{R}\arctan\left(\frac{R}{R_c}\right)\right]$$

with an asymptotic maximum velocity of

$$V_\infty = \sqrt{4\pi G\rho_0 R_c^2}$$

In the context of the disk-halo conspiracy, the value of V_∞ is equivalent to the amplitude of the flat part of the rotation curve. Most of the observed declining rotation curves reach a flat part in their outer regions. (So far, no rotation curves have been observed which unambiguously and significantly turn up after they remained flat over an extended radial interval.) Note that the slope

of this halo rotation curve at the center is related to the central core density and the ratio of the asymptotic velocity and the core radius like

$$\left(\frac{\partial V_{\rm halo}}{\partial R}\right)_{R=0} = 1.15\sqrt{\pi G\rho_0} = 0.577\,\frac{V_\infty}{R_c}$$

The total mass of the isothermal sphere halo does not converge when integrating the density profile to infinity. The effect of an adiabatic compression of the dark matter due to the baryons in the center can be partly accommodated by a smaller value of the core radius.

b) The Hernquist profile

An often used alternative to the isothermal sphere model is a density profile introduced by Hernquist (1990) to allow for an analytic treatment of the density profiles in bulges and ellipticals. This Hernquist model is described by

$$\rho(R) = \frac{M_0}{2\pi R_0^2}\frac{1}{R\left(1+\frac{R}{R_0}\right)^3} = \frac{\Sigma_0}{R\left(1+\frac{R}{R_0}\right)^3}$$

where M_0 is the total mass of the halo and R_0 an effective truncation radius. Σ_0 can be considered as a global surface density of the dark matter halo. The mass enclosed by a circular orbit of radius R is given by

$$M(R) = M_0\left(\frac{R}{R+R_0}\right)^2 = 2\pi\Sigma_0 R_0^2\left(\frac{R}{R+R_0}\right)^2$$

which gives rise to a rotation curve of the form

$$V_{halo}(R) = \frac{\sqrt{GM_0R}}{R+R_0}$$

which reaches its maximum at $R = R_0$ of

$$V_{halo}^{max} = 1039\sqrt{\frac{M_0}{R_0}} \quad \text{(km/s)}$$

where M_0 is in $10^{12}M_\odot$ and R_0 is in kpc.

The shape of this halo rotation curve is nearly identical to the shape found by Navarro *et al* over the radial range where galactic rotation curves can be measured. Differences can only be expected in the very inner regions where the luminous matter in general dominates and near the outer truncation radius R_0 where rotation curves have not been measured so far.

5 The decompositions

From the 30 unperturbed rotation curves (Table 1) the 22 curves with at least five measured points were modelled by a 3-component fit:

$$V_{\rm mod}^2(r) = V_{\rm disk}^2(r) + V_{\rm gas}^2(r) + V_{\rm halo}^2(r)$$

where $V_{\rm disk}$ is the rotational velocity induced by the potential of the stellar disk, $V_{\rm gas}$ the velocity induced by the potential of the gas and $V_{\rm halo}$ is the rotational velocity of the dark matter halo as given in the previous section.

The gravitational potential induced by the stellar component is derived directly from the observed luminosity profiles. No attempt was made to decompose these luminosity profiles into a disk and a bulge component in cases where the luminosity profile shows an upturn near the center. The angular resolution with which the rotation curves were observed does not allow one to make a clear distinction between the quadratic sum of a bulge and a disk rotation curve and a single rotation curve arising from a disk with an enhanced central density. When constructing the potential from the (possibly non-)exponential disk, we assume that all the stars are located in a disk with a vertical sech^2 distribution of scale height z_0=0.2r_d (van der Kruit and Searle, 1981) where r_d is the exponential disk scale length fitted to the quasi linear part of the luminosity profiles. The shape of $V_{\rm disk}$(r) is calculated from the K′-band luminosity profiles, presented in Chapter 1, using the prescription by Casertano (1983) and Begeman (1987). Since the I-band profiles could be measured to larger radii and galaxies are nearly transparent in their outer regions, the K′-band profiles were extended with the up-scaled I-band profiles. The amplitude of $V_{\rm disk}$(r) scales with the mass of the stellar disk like $\sqrt{M_{\rm disk}}$. The mass $M_{\rm disk}$ is calculated from the total absolute K′ magnitude $M_{K'}$ and the stellar K′-band mass-to-light ratio $M/L_{K'}$ according to

$$M_{\rm disk} = (M/L_{K'}) \times 10^{-0.4(M_{K'}-3.41)} \quad (M_\odot)$$

where 3.41 is the adopted solar absolute K′ magnitude (Allen, 1973). It is assumed that $(M/L_{K'})$ does not change with radius. A purely exponential disk with face-on central surface brightness μ_0^i(K′) mag/arcsec^2, scalelength r_d (arcsec) and stellar mass-to-light ratio $M/L_{K'}$ reaches, at 2.1r_d, its maximum rotational velocity in km/s of

$$V_{\rm disk}^{\rm max} = 8.60\times10^4\sqrt{(M/L_{K'})\,10^{-0.4\,\mu_0^i({\rm K'})}\,r_{d({\rm K'})}}$$

The rotation curve of the gaseous component is calculated from the radial HI surface density profile, mul-

tiplied by 1.32 to account for the mass fraction of helium. It is assumed that the gas resides in an infinitely thin disk. The mass of the gas disk is fixed given the integrated HI flux by

$$M_{\rm gas} = 1.32 \times 2.36 \times 10^5 D^2 \int S_v dv \quad (M_\odot)$$

where D is the distance in Mpc and $\int S_v dv$ the integrated HI flux in Jy km/s. We adopt a common distance of D=15.5 Mpc for all galaxies in our cluster sample.

When fitting the models described above to the observed rotation curves, there are three model parameters to be determined. These are the mass-to-light ratio of the stellar disk, the core radius R_c and the asymptotic rotational velocity V_∞ for the isothermal sphere model, or alternatively the halo mass M_0 and radius R_0 for the Hernquist model. A χ^2–minimalization analysis using all three parameters shows a very broad and noisy minimum. For instance, most observed rotation curves can be well fitted by a halo rotation curve alone. Therefore, we reduced the number of free parameters in our fits by fixing the mass-to-light ratio of the stellar disk while fitting the two halo parameters. In fact, the inferred structure of the dark matter halo derived from its fitted parameters depends strongly on the assumed stellar mass-to-light ratio. When comparing the structural parameters of dark matter haloes of different galaxies it should be noted that galaxy-to-galaxy variations in the mass-to-light ratio of the stellar populations may create or destroy spurious trends. To minimize this potential problem we considered the stellar mass-to-light ratios in the K'–passband which depend less on the properties of the stellar populations (like its age and metallicity) than the mass-to-light ratios in the optical passbands.

The observed rotation curves were decomposed in four different ways with various assumptions about the K' stellar mass-to-light ratio. The decompositions are presented graphically in the appendix. For each galaxy eight panels are plotted. The four left hand panels ($*1$) show the decompositions with an isothermal sphere. The four right hand panels ($*2$) present the decompositions with a Hernquist halo. Panels a$*$ show the results for a maximum-disk fit. Panels b$*$ present the decompositions assuming that the luminous mass in the HSB galaxies provides 63% of the maximum observed rotational velocity (Bottema, 1993). The corresponding mass-to-light ratios of the HSB galaxies were averaged and the value thus obtained was used for the LSB galaxies. The decompositions shown in panels c$*$ were made by assuming that all galaxies have the same near-infrared mass-to-light ratio of 0.6. Finally, in panels d$*$, the M/L was fitted assuming that the disk-halo conspiracy holds until the halo rotation curve reaches its maximum velocity. For the isothermal sphere it was therefore assumed that $V_\infty = V_{\rm flat}$ and for the Hernquist halo it was assumed that $V_{max} = 0.5\sqrt{GM_0/R_0} = V_{\rm flat}$ which fixes the ratio between M_0 and R_0. In the following subsections, each method will be addressed in somewhat more detail.

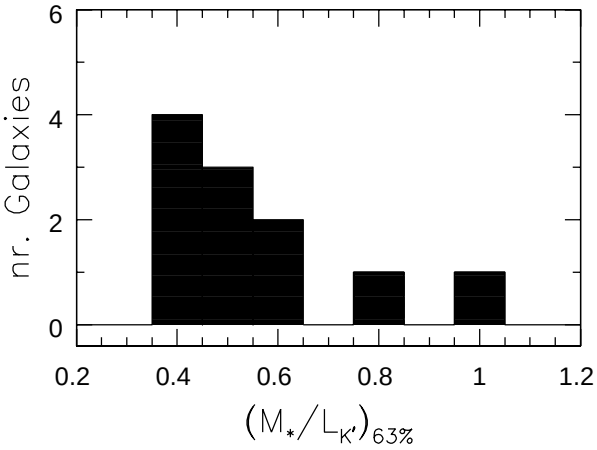

Figure 8: Distribution of stellar K' mass-to-light ratios assuming that the stellar disk contributes 63% to the observed maximum rotational velocity.

5.1 Maximum-disk fits

Maximum-disk fits were made by assuming a maximum contribution of the luminous matter to the gravitational potential. This provides a lower limit on the amount of dark matter inside the observed baryonic part of the galaxy. For each galaxy the stellar mass-to-light ratio was maximized in such a way that the rotational velocities induced by the luminous mass were as high as possible without exceeding the observed rotational velocities. As a result, the rising rotation curve of the dark matter halo in the inner regions is flattened and 'pushed outward'.

For the isothermal halo, this results in large core radii and a halo rotation curve which is often still rising just beyond the last measured point. The latter aspect suggests that in those cases the observed apparent disk-halo conspiracy would break down if the HI disk would have been slightly more extended. No rotation curves have been observed that show a sudden upturn at their last measured points. Therefore, an additional soft constraint on the maximum mass-to-light ratio was invoked by demanding that the fitted V_∞ of the isothermal sphere does not deviate by more than 10% from the amplitude of the flat part of the observed rotation curve.

5.2 'Bottema-disk' fits

One of the few more direct ways to measure the mass-to-light ratio is via stellar velocity dispersions in spiral galaxies with a self-gravitating stellar disk. From these kind of observations, Bottema (1993) concluded that the maximum rotational velocity induced by the stellar disk contributes on average about 63% to the observed maximum rotational velocity. In this spirit, we adjusted the stellar mass-to-light ratios in our HSB galaxies such that the corresponding V_{disk}^{max} is 63% of V_{obs}^{max}. Figure 8 shows the distribution of the M/L ratios found in this way. Excluding the two extreme cases (N3972 and N3992), we find for nine galaxies an average value of $(M_*/L_{K'})$=0.46 with a scatter of 19%. Assuming that the near-infrared mass-to-light ratios in LSB galaxies are similar to those in HSB systems, we adopted this representative value when decomposing the rotation curves of the low surface brightness galaxies.

5.3 Equal ($M_*/L_{K'}$) fits

We also derived the structural properties of the haloes by assuming that the different stellar populations have the same near-infrared ($M_*/L_{K'}$) in all galaxies. This approach might not be too ridiculous since the ($M_*/L_{K'}$) of a stellar population is less affected by age, metallicity and star formation history than the mass-to-light ratios in the optical passbands. We chose a value of $(M_*/L_{K'})$=0.60 for all galaxies, which is a compromise between the median value of 0.78 given by the maximum-disk fits of the HSB galaxies and the minimum maximum-disk value of 0.30 (N4085). Consequently, the adopted value of 0.60 could result in unrealistic run-away halos with values for V_∞ that are too large. The actual datapoints, however, are not seriously exceeded. In the case of N3992, the support by the luminous matter is much too small with $(M_*/L_{K'})$=0.60 and the halo required to explain the observed rotation curve would have a core radius of 10 pc and a central density of 15×10^3 $M_\odot pc^{-3}$ which seems quite unrealistic. For the two galaxies in which the soft constraint on V_∞ for the maximum-disk fits gets violated, the fits still seem acceptable although the value of V_∞ for the halo of N4085 is a bit high.

5.4 'Constrained-halo' fits

So far, we have been fitting the two structural parameters of the halo (i.e. (R_c,V_∞) for the isothermal sphere and (R_0,M_0) for the Hernquist halo) while keeping the ($M_*/L_{K'}$) fixed at educated-guess values. Finally, we also attempted to derive ($M_*/L_{K'}$) values by making fits to the rotation curves while keeping one of the structural parameters of the halo fixed.

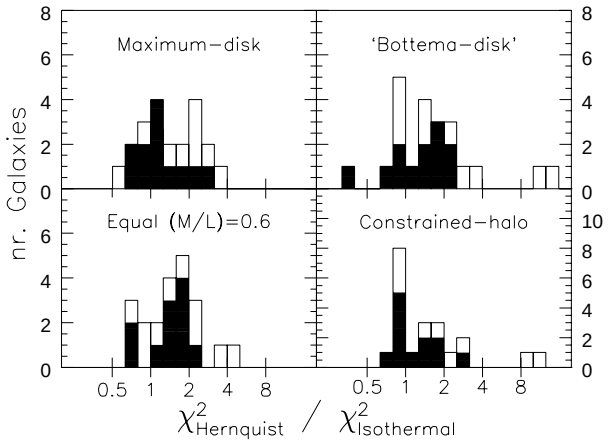

Figure 9: Distributions of the ratios of χ^2 from the fits using a Hernquist profile and an isothermal sphere model. In both cases, the same number of parameters were fitted. Distributions are shown for the various fitting methods. The solid histogram corresponds to the HSB galaxies and the open histogram to the LSB galaxies. In general, the isothermal sphere model gives relatively smaller χ^2 values than the Hernquist model, i.e. $(\chi^2_{Hernquist}/\chi^2_{isothermal})>1$.

Searching for a constraint on one of the halo structural parameters, the phenomenology of the disk-halo conspiracy in the outer parts of rotation curves gives a useful clue. We make the assumption that this disk-halo conspiracy also holds at large radii where the amplitude of the rotation curve is completely determined by the dark matter halo. Consequently, the maximum rotational velocity induced by the dark matter halo should be equal to the amplitude of the observed flat part of a rotation curve. For an isothermal sphere this implies that $V_\infty=V_{flat}$ and for an Hernquist halo it means that $V_{halo}^{max}=0.5\sqrt{GM_0/R_0}=V_{flat}$ or

$$M_0\ [10^{10}M_\odot] = R_0\ [kpc]\ \left(\frac{V_{flat}[km/s]}{103.9}\right)^2$$

With this relation we can express the shape of the rotation curve of the Hernquist halo in terms of R_0 and V_{flat} and decompose the observed rotation curves by fitting ($M_*/L_{K'}$) and R_0 while keeping V_{flat} fixed at its observed value.

It turns out that the ($M_*/L_{K'}$) values found in these constrained-halo fits are quite similar to the maximum-disk values, both for the isothermal sphere and the Hernquist halo. This result is not entirely obvious since unconstraining the stellar M/L ratio gives the fitting algorithm much freedom within the broad and noisy χ^2-minimum to make a trade-off between the halo core

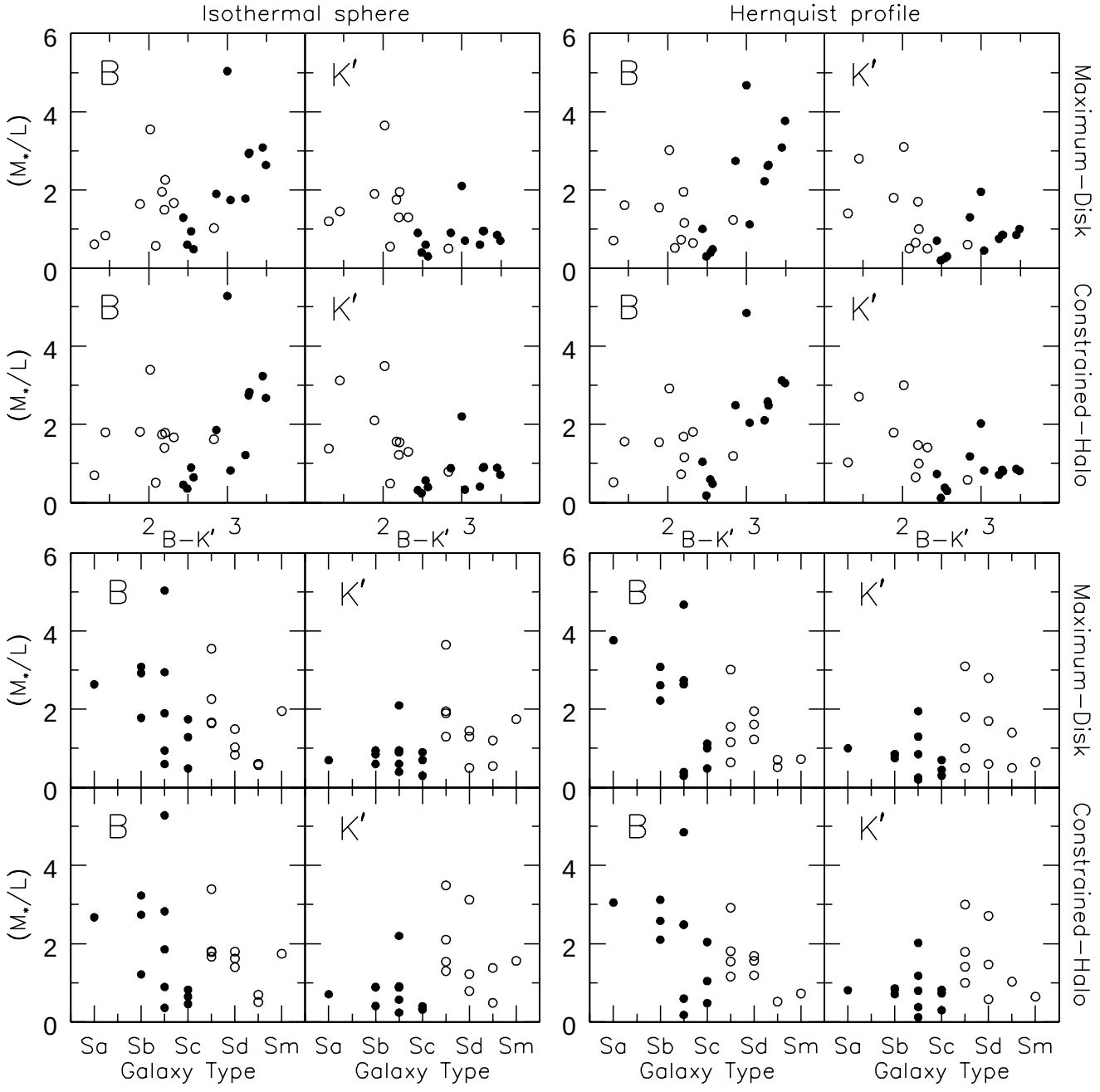

Figure 10: Trends in stellar B and K' mass-to-light ratios as a function of color and morphology. An isothermal sphere was used to obtain the results in the left two blocks and a Hernquist profile was used to obtain the results in the right two blocks. Mass-to-light ratios in the upper two panels of each block were obtained from maximum-disk fits and mass-to-light ratios in the lower two panels of each block were obtained from constrained-halo fits. Filled symbols: HSB galaxies. Open symbols: LSB galaxies.

radius and the mass-to-light ratio. Apparently, the observed shapes of the rotation curves in the inner regions are such that a maximum-disk situation is preferred instead of a maximum-halo solution with a small core radius.

No converging solution could be found for U6923 in case of the Hernquist halo. This galaxy has the least number of observed points (6) along its rotation curve.

6 Results from the decompositions

In this section we will discuss the results obtained from the various decompositions. Mass-to-light ratios and the structural parameters of the haloes are collected in Tables 2a and 2b in the appendix which also contains graphical representations of the decompositions.

To evaluate whether the Hernquist profiles give better fits to the observed rotation curves than the isothermal sphere models, we calculated χ^2_{red} for each fit. For both halo models, the same number of parameters were fitted to the same data points. If both models gave equally good or bad fits, we would expect comparable values for the two χ^2_{red} and their ratio should be close to unity. This ratio does not tell us whether a particular pair of fits is intrinsically good or bad but it gives a clue about their relative successes. The distribution of these ratios is plotted in Figure 9 for each of the four decomposition methods. The filled histograms show the distributions for the HSB galaxies and the open histograms those of the LSB galaxies. We see that, in a statistical sense, the Hernquist models give larger values of χ^2_{red} than the isothermal sphere models. Of course, more sophisticated statistical tests should be applied but these will be postponed until later. For the moment, Figure 9 gives a first hint that the isothermal sphere models give tighter fits to the observed rotation curves than the Hernquist models.

6.1 Mass-to-light ratios

The stellar mass-to-light ratios were allowed to vary from galaxy-to-galaxy for the maximum-disk and the constrained-halo fits. Therefore, these fits allow us to investigate whether trends in the stellar mass-to-light ratio are present as a function of color and morphological type for instance. Mass-to-light ratios could also be investigated as a function of luminosity and rotational velocity but all these properties are more or less correlated along the Hubble-sequence. Figure 10 shows results for both the isothermal sphere model and the Hernquist model. The filled symbols indicate HSB galaxies and the open symbols correspond to LSB systems. The maximum-disk mass-to-light ratios are also constrained by the shapes of the luminosity profiles in the inner regions. Recall that the fits were made by using the K' luminosity profiles which were extended with the *I*-band profiles in the outer regions. Figure 10 presents K'-band mass-to-light ratios as well as *B*-band (M/L) values. These latter ones were not obtained by making separate fits with the *B*-band luminosity profiles but were calculated from the fitted K' mass-to-light ratios according to

$$\left(\frac{M_*}{L_B}\right) = \left(\frac{M_*}{L_{K'}}\right) \times \frac{10^{-0.4(M_{K'}-M_{K',\odot})}}{10^{-0.4(M_B-M_{B,\odot})}}$$

where $M_{K',\odot}$=3.41 and $M_{B,\odot}$=5.46 are the adopted absolute magnitudes of the Sun.

The first thing to be appreciated from Figure 10 is that the results from maximum-disk fits and those of the constrained-halo fits are quite consistent with each other for both the isothermal sphere model and the Hernquist model. Considering the constrained-halo fits, it is obvious that, for an isothermal sphere, the core radius and the mass-to-light ratio are strongly coupled: larger values of M/L push the core radius further outward. For the Hernquist model, such a correlation between M/L and the truncation radius R_0 is less clear but nevertheless present.

We find that the K' mass-to-light ratios of the HSB galaxies are independent of color and morphological type, and above all, their values lie typically between 0.4 and 1.0, a very reasonable range. This observation gives strong support to the maximum-disk hypothesis in high surface brightness galaxies. Since the K' (M/L)-values of the HSB galaxies are independent of color we find a significant correlation of the *B*-band (M/L)-values as a function of color given the conversion from K' to *B*-band mass-to-light ratios as explained above. Furthermore, the mass-to-light ratios of the HSB galaxies show a much smaller scatter than those of the LSB galaxies. A detailed comparison with stellar population synthesis models seems an obvious topic for future study.

6.2 Correlations between luminous mass and halo parameters

In this section we investigate possible correlations between the structural parameters of the dark matter haloes and their relation to the distribution of the luminous matter. For the moment we will restrict ourselves to the isothermal sphere model only and review its structural parameters as derived from fits to the observed rotation curves with equal K' mass-to-light ratio of $(M_*/L_{K'})$=0.6 for all galaxies. In practice the values of the core radius R_c and the asymptotic maximum velocity V_∞ were fitted without any constraints while keeping $(M_*/L_{K'})$ fixed at the specified value. The central halo density ρ_0 was calculated from (R_c,V_∞) ac-

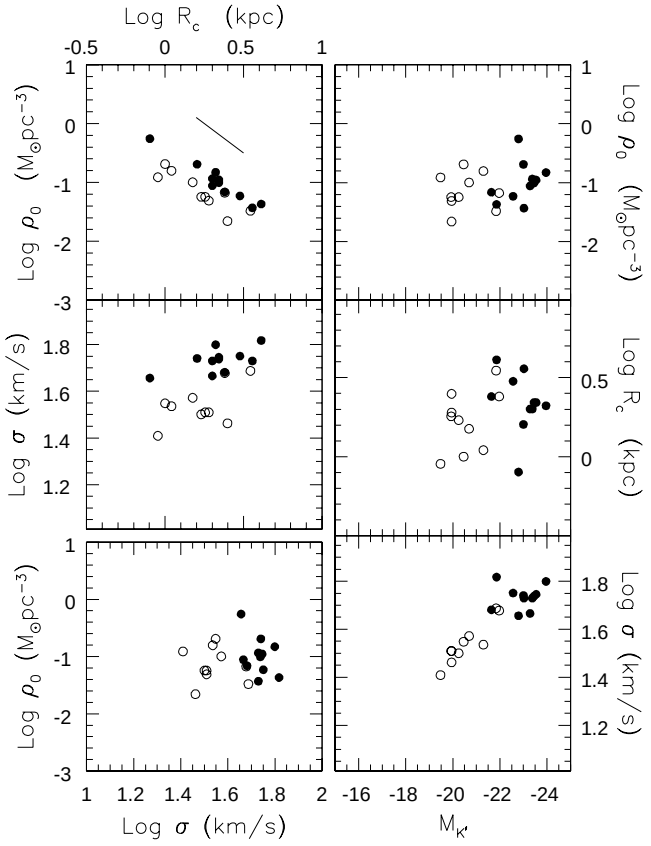

Figure 11: Correlations between the structural parameters of the isothermal sphere and their relations to the K' luminosity. Equal ($M_*/L_{K'}$)=0.6 for all galaxies was assumed.

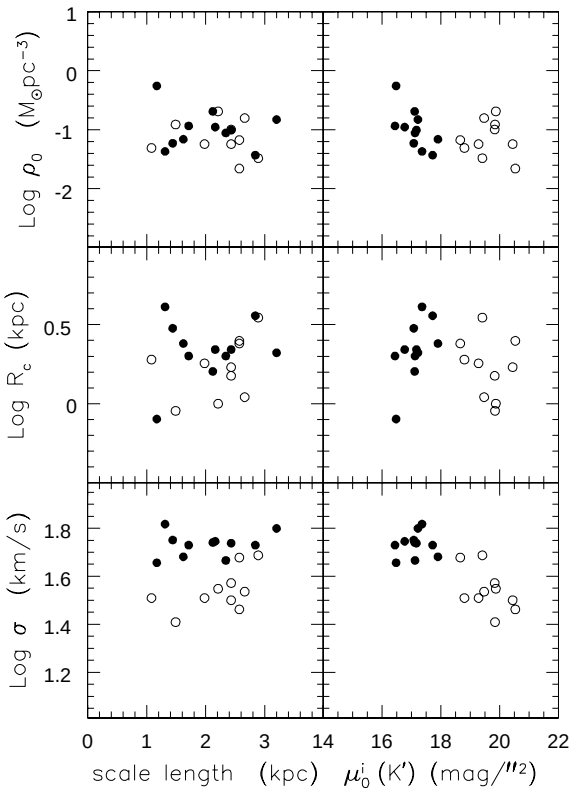

Figure 12: Correlations between the structural parameters of the isothermal spere and the scale length and central disk surface brightness. Equal ($M_*/L_{K'}$)=0.6 for all galaxies was assumed.

cording to $\rho_0=V_\infty^2/4\pi GR_c^2$ and a velocity dispersion σ of the halo was calculated according to $\sigma=\frac{1}{3}V_\infty$.

The left hand panels of Figure 11 show the correlations among the structural parameters plotted in a similar fashion as Kormendy's (1990) relations. The apparently obvious anti-correlation between ρ_0 and R_c is partially an artifact since ρ_0 follows from R_c and V_∞. The line drawn in this panel indicates how ρ_0 is affected if R_c changes by a factor of 2. This can easily occur for small changes in (M/L) close to a maximum-disk situation; i.e., if M/L is lowered then the halo draws in to smaller R_c to compensate. The line has the same slope as the correlation. With the specified value of (M/L)=0.6, the HSB galaxies are often close to this maximum-disk situation while the LSB galaxies are far below maximum-disk. For the LSB galaxies, therefore, the correlation between R_c and ρ_0 is genuine provided that indeed (M/L)=0.6 for these systems, which results in an almost irrelevant potential of the luminous component. The fact that the LSB galaxies (open symbols) are systematically offset from the HSB galaxies (filled symbols) should not raise any concern since lines of constant log(σ) also have a slope of -2 and run parallel to each other. Hence, the 'offset' between HSB and LSB galaxies is simply related to their different rotational velocities. Our data suggest a weak correlation between velocity dispersion and core radius (middle left panel) in the sense that more massive haloes have larger core radii. In the lower left panel we find no relation between velocity dispersion and central density.

The right hand panels show basically the same trends between near-infrared luminosity and ρ_0 or R_c as found between σ and ρ_0 or R_c because $M_{K'}$ and σ are correlated via the TF-relation. Its equivalent is plotted in the lower right panel. We find no significant correlation of $M_{K'}$ with ρ_0 and at most a marginal correlation with R_c.

In Figure 12 we check for possible correlations between the halo parameters and the disk scale lengths and central surface brightness. From the upper left panel we conclude that there is no correlation between central halo density and the disk scale length. The mid-

dle left panel suggests that at a given disk scale length, LSB galaxies have smaller core radii. The apparent offset in the lower left panel is again related to the TF-relation. There is no correlation between disk scale lengths and rotational velocities. Correlations between the central disk surface brightness and central halo densities or core radii are at most marginal. The correlation between velocity dispersion and surface brightness represents again the TF-relation since surface brightness is strongly correlated with luminosity in our sample.

We end this section by recalling that these results were obtained from decompositions assuming equal mass-to-light ratios for all galaxies. It should be noted that maximum-disk decompositions may result in very different scaling relations and may even show strong artificial correlations. Nevertheless, under the assumption of equal ($M_*/L_{K'}$)=0.6 for all galaxies, which leads to a maximum-disk situation for most HSB systems, there is no hint of the hierarchical clustering expectation that ρ_0 is larger for low luminosity galaxies. However, we have probed only a limited range in mass.

6.3 Dark to luminous mass fractions

We calculated the total amounts of dark matter within the last measured points of the rotation curves M_{dark}^{lmp} according to

$$M_{dark}^{lmp} = 4\pi\rho_0 R_c^2 \left[R^{lmp} - R_c \mathrm{atan}\left(\frac{R^{lmp}}{R_c}\right)\right]$$

for the isothermal halo and according to

$$M_{dark}^{lmp} = M_0 \left(\frac{R^{lmp}}{R^{lmp}+R_0}\right)^2$$

for the Hernquist halo. The dark matter masses calculated in this way are of course model dependent. It should be noted that the fraction of luminous to dark mass does depend on the radius at which the last point on the rotation curve was measured. In general, nearly all of the light is enclosed within this radius so the stellar mass M_{stars} will not increase significantly when going to larger radii. Of course, M_{stars} does depend on the adopted value of the stellar (M/L). For a flat rotation curve, however, M_{dark} will still increase with radius. For an isothermal sphere, $M_{dark}/M_{lum} \propto R$ once R is large enough to enclose all the luminous mass. Consequently, mass fractions determined within the last measured points have a limited meaning. This is further stressed by the insets of Figure 1 which illustrate that, for galaxies of similar luminosities, the radii of the last measured points can easily differ by a factor of five, both in terms of kiloparsec and in disk scale lengths.

Nevertheless, let us consider the relative amounts of mass represented by each of the three dynamical constituents of a spiral galaxy. As mentioned above, the amount of mass locked-up in the stars M_{stars} depends of course on the adopted mass-to-light ratio. The mass of the gaseous component M_{gas} is calculated from the observed HI line flux, multiplied by 1.32 to correct for the amount of helium. The mass of the dark matter component M_{dark} is calculated from the fitted model as explained above. We calculated the total mass of the luminous matter as $M_{lum}=M_{stars}+M_{gas}$. Figures 13 and 14 show the various mass fractions as a function of the amplitude of the flat part of the rotation curves. Given the TF-relation, the abscissa can also be interpreted as K' luminosity. In Figure 13, M_{stars} and the halo parameters were obtained by assuming equal mass-to-light ratios for all galaxies. In Figure 14, the relevant parameters were obtained from constrained-halo fits. The filled symbols correspond to the HSB galaxies in our sample and the open symbols relate to the LSB galaxies.

The upper panels show the M_{gas}/M_{stars} ratio which depends on the adopted or fitted mass-to-light ratio. Independent of fitting method and halo model we observe the well known trend that M_{gas}/M_{stars} increases with decreasing mass or luminosity. A large fraction, if not most, of the baryonic mass content of dwarf galaxies is in a gaseous form. The second row of panels shows the M_{gas}/M_{dark} ratio which follows the same trend with luminosity as the M_{gas}/M_{stars} ratio. In dwarf galaxies the amount of mass in the form of gas may be as much as 10-20% of the amount of mass in the dark matter component. In the third row of panels we plot the ratio of M_{stars}/M_{dark} and run into an unfortunate situation. When considering the equal-(M/L) fits we should conclude that the relative amount of mass locked-up in the stars decreases with decreasing luminosities, independent of the adopted halo model. However, when considering the constrained-halo fits one would reach exactly the opposite conclusion in the case of an isothermal sphere model. When adopting the Hernquist density profile for the dark matter halo, the constrained-halo fits seem to indicate that the M_{stars}/M_{dark} ratio is nearly constant with luminosity albeit with a large scatter. Adding M_{gas} to M_{stars} and plotting the M_{lum}/M_{dark} ratios in the lower panels creates an even more unfavorable situation. We are forced to conclude that trends in the M_{lum}/M_{dark} ratios depend on the fitting method.

It is very desirable to obtain independent and more direct determinations of the mass-to-light ratios of stellar populations in spiral galaxies, for instance via stellar velocity dispersions.

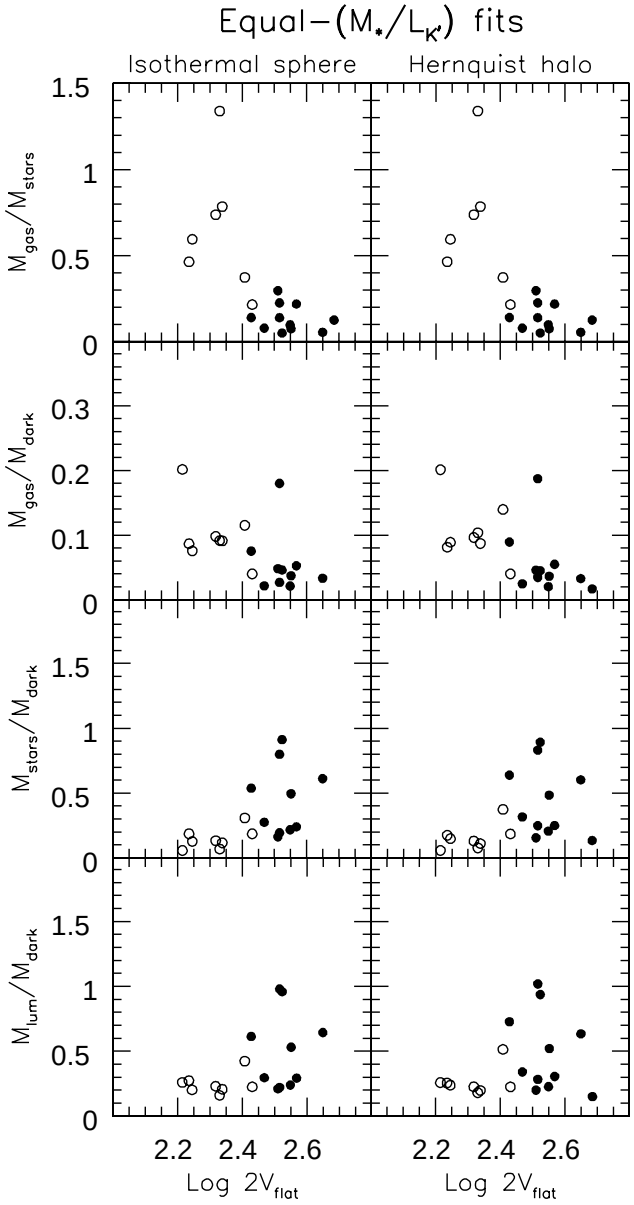

Figure 13: Mass ratios between the three dynamical components of a spiral galaxy determined within the last measured point on the rotation curve. The stellar mass was calculated from the stellar K' mass-to-light ratio which was assumed to be equal for all galaxies. The masses of the dark matter were calculated from the models using the fitted structural parameters.

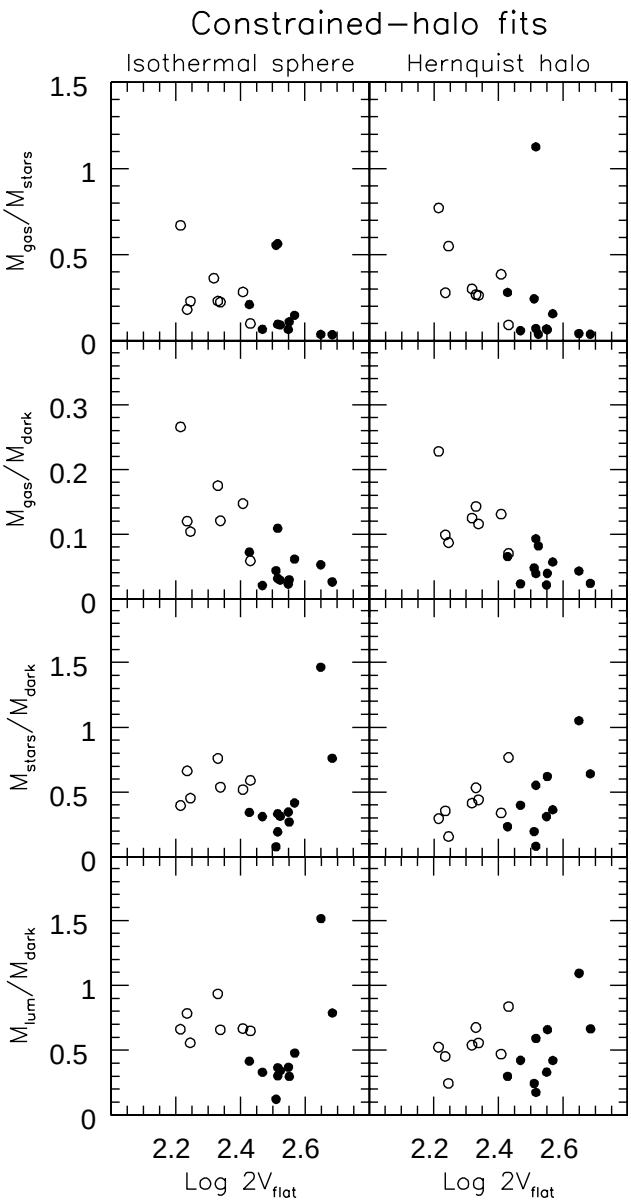

Figure 14: Mass ratios between the three dynamical components of a spiral galaxy determined within the last measured point on the rotation curve. The stellar mass was calculated from the stellar K' mass-to-light ratio which was obtained from the constrained-halo fits. The masses of the dark matter were calculated from the models using the fitted structural parameters.

7 A kinematic bimodality?

In Chapter 3 we investigated the distributions of the extrapolated central disk surface brightnesses in the *B*, *R*, *I* and K' passbands. It turned out that the face-on K' central surface brightness $\mu_0^i{}_{(K')}$ has a bimodal distribution. The stellar disks in spiral galaxies seem to avoid central surface brightnesses around $\mu_0^i{}_{(K')}$=18.5 mag. It was then anticipated that such a bimodal distribution may also have a kinematic signature. This idea is based on the fact that the rotation curve of an exponential disk peaks near $2.1r_d$ and that for galaxies of the same luminosity, this peak velocity is proportional to the surface brightness. The observation

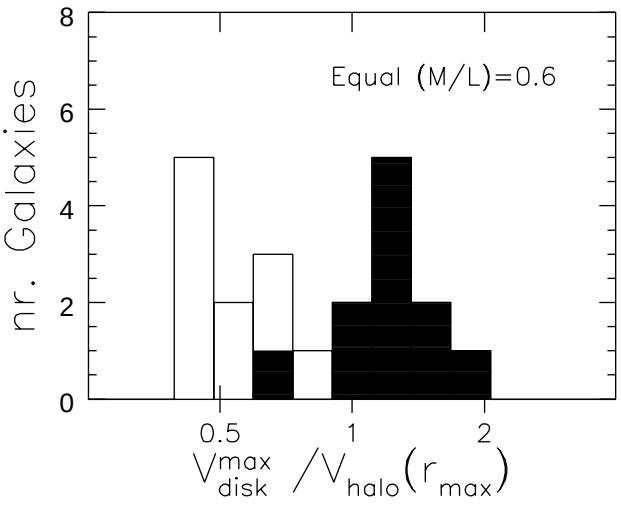

Figure 15: Distribution of ratios between the maximum rotational velocity V^{max}_{disk} induced by the potential of the disk and the rotational velocity $V_{halo}(r_{max})$ of the isothermal dark matter halo at the radius r_{max} where V^{max}_{disk} occurs. When calculating V^{max}_{disk}, equal values of $(M/L_{K'})$=0.6 for all galaxies was assumed. The filled histogram indicates the distribution for HSB galaxies and the open histogram that for the LSB galaxies. N3992 is omitted because of the unacceptable fit for (M/L)=0.6 .

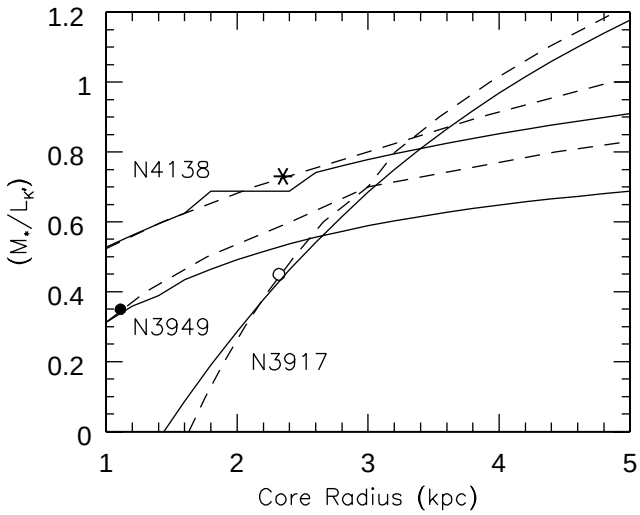

Figure 16: Correlation between fitted mass-to-light ratio and core radius for three galaxies of similar luminosity but with different distributions of the luminous matter.

that galaxies of the same luminosity but with different surface brightnesses lie at the same position on the TF-relation suggests that a bimodal distribution of surface brightnesses translates into a bimodal distribution in the $V^{max}_{disk}/V^{max}_{obs}$ ratio. It was argued that HSB galaxies have self-gravitating disks and LSB disks are dynamically dominated by the dark matter halo. In the first case one would expect V^{max}_{disk} to exceed the rotational velocity of the halo $V_{halo}(r_{max})$ at the radius r_{max} where the disk rotation curve peaks. In the latter case one would expect that the rotation curve of the dark matter halo at r_{max} exceeds the peak rotational velocity induced by the stellar disk.

We measured the $V^{max}_{disk}/V_{halo}(r_{max})$ ratios by assuming an equal K' mass-to-light ratio of 0.6 and an isothermal dark matter halo. Figure 15 shows the results. Although we are dealing here with less galaxies than in Chapter 3, a certain bimodality seems evident with a minimum very near to $(V^{max}_{disk}/V_{halo}(r_{max}))$ = 1. In general, the $V^{max}_{disk}/V_{halo}(r_{max})$ ratio is larger than unity for the HSB galaxies and lower than unity for LSB galaxies. This indicates that the disk rotation curves of HSB systems exceed the dark matter rotation curve at the radius where V_{disk} peaks, a condition indicative of a self-gravitating disk. For LSB galaxies, the peak velocity of V_{disk} reaches on average only half the rotational velocity of V_{halo} at the corresponding radius, a condition indicative of a halo-dominated potential. This result does not change if one considers a Hernquist halo instead of an isothermal sphere. It should be noted, however, that the rotational velocity of the other baryonic component, the gas disk, was neglected. Inclusion of this component into V_{disk} to obtain V_{baryon} would shft the distribution a bit further to the right.

8 Haloes of HSB and LSB galaxies

The question whether HSB and LSB galaxies of the same luminosity are located in similar haloes has been a subject of some debate in recent years (e.g. de Blok and McGaugh 1996) and this issue is directly related to understanding the process of galaxy formation. It was shown in Chapter 5 and by Zwaan *et al* (1995) that LSB galaxies follow the TF-relation defined by HSB spirals which implies that the TF-relation is a correlation between luminosity and the velocity dispersion of the dark matter. By comparing the rotation curves of the HSB/LSB-pair NGC2403/UGC128 de Blok and McGaugh (199) concluded that the structural properties of the haloes around these two galaxies are different. The LSB galaxy U128 is surrounded by a halo with a lower central density and a larger core radius than its HSB counterpart. In this section we intend to investigate whether this result can be verified with our observations.

In our sample of Ursa Major spirals with available

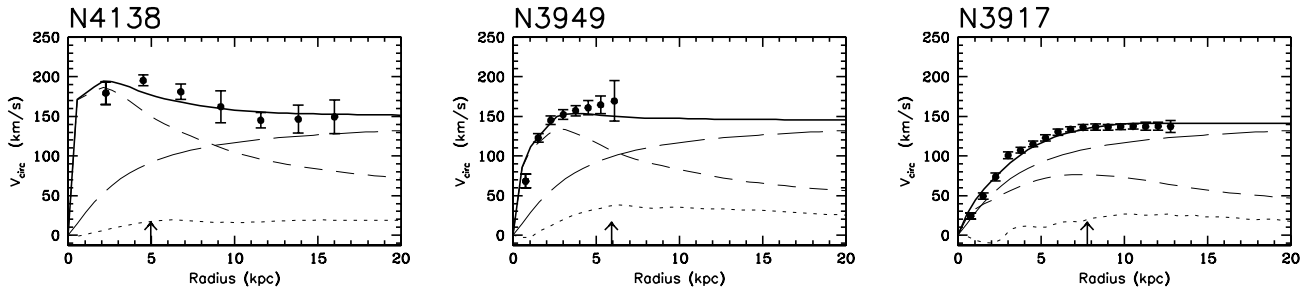

(a) $(M_*/L_{K'})$=0.8 (b) $(M_*/L_{K'})$=0.6 (c) $(M_*/L_{K'})$=0.7

Figure 17: Rotation curve decompositions for three galaxies of the same luminosity but with different central disk surface brightnesses. Identical haloes with V_∞=149 km/s and R_c=3 kpc (long dashed lines) for all three galaxies were assumed. Only minor differences in mass-to-light ratio allow for acceptable fits. The vertical arrows indicate R_{25}.

HI rotation curves, the overlap in luminosity between HSB and LSB galaxies is limited. Fortunately, we can identify three galaxies with nearly the same luminosities but with different distributions of the luminous mass:

name	M_B (mag)	$M_{K'}$ (mag)	$\mu^i_0(K')$ (mag/$''^2$)	r_d (kpc)	C_{82}
N3917	-19.65	-21.97	18.66	2.6	3.0
N3949	-20.07	-22.56	17.08	1.4	3.7
N4138	-19.70	-22.79	16.48	1.2	5.3

The central surface brightness of N3917 is quite high for an LSB system and in fact this system lies very close to the K' surface brightness limit which we adopted in Chapter 3 when defining the HSB and LSB families of galaxies. The relative positions of these three galaxies on the TF-relation is illustrated in Figure 7 of Chapter 5.

We examine now the structural properties of the haloes that surround these three galaxies. We are especially interested in the central densities and core radii of their haloes. We decomposed their rotation curves by fitting the core radii and the stellar mass-to-light ratios while keeping the maximum asymptotic velocity of the assumed isothermal sphere halo fixed. The fixed value of V_∞=149 km/s was taken as the average of the observed amplitudes of the outer flat parts of the three rotation curves (135, 164 and 147 km/s). Figure 16 shows the results from fitting the stellar mass-to-light ratio and the halo core radius R_c for each of the three galaxies. The three symbols indicate the results when fitting M/L and R_c simultaneous as free parameters. The solid lines indicate for each galaxy how the fitted M/L values vary as a function of core radius when keeping both V_∞=149 km/s and R_c fixed at the specified values. The dashed lines show how R_c varies as a function of M/L when keeping both V_∞=149 km/s and M/L specified. The symbols indicate the positions of the minimum of χ^2 along each of the paired lines. Figure 17 shows that if one adopts the same halo with a core radius of 3 kpc for all three galaxies, acceptable fits are obtained for K' mass-to-light ratios of 0.8, 0.6 and 0.7 for N4138, N3949 and N3917 respectively. This is only a small range.

In conclusion, the observed rotation curves of these three galaxies of the same luminosity but with different distributions of their stellar components are consistent with the hypothesis that they are surrounded by identical haloes under the assumption that the stellar populations of these three galaxies have nearly the same K' mass-to-light ratio. In other words, they would have the same halo and similar $(M_*/L_{K'})$ and be left free to distribute their luminous mass.

9 Conclusions

In this chapter we analyzed the shapes of HI rotation curves of 30 spiral galaxies located in the nearby Ursa Major cluster. Since all the galaxies are nearly at the same distance there is little doubt about their relative luminosities, sizes and masses. The 22 rotation curves with at least five measured points were decomposed into the three dynamical constituents of a spiral galaxy: the stellar, gas and halo component. We adopted alternatively an isothermal sphere and a Hernquist model to describe the density profile of the dark matter halo. Maximum-disk, equal-$(M_*/L_{K'})$ and constrained-halo decompositions were performed. Our main conclusions are the following:

- The shapes of rotation curves correlate with the compactness of the stellar component in the

sense that for galaxies of the same luminosity, a more compact distribution gives rise to a steeper rotation curve. Occasionaly, when the maximum rotational velocity exceeds ≈150 km/s, rotation curves may be declining in the outer parts. Our findings are in accordance with those of Casertano and Van Gorkom (1991).

- We find that about one third of our observed rotation curves do not have the 'universal rotation curve' shape.

- In maximum-disk fits and constrained-halo fits for HSB galaxies the derived K' mass-to-light ratios are independent of color and morphological type and display a relatively small scatter. In the case of maximum-disk fits for LSB galaxies we find that (M/L) requirements are systematically much higher than in the HSB cases and there is a much larger scatter in the (M/L) values. The small scatter in the fits for the HSB cases is evidence that the maximum disk hypothesis is roughly justified for HSB systems. The large (M/L) requirement and large scatter in the fits for LSB cases is evidence that the maximum disk hypothesis fails for LSB systems.

- The structural parameters of dark matter haloes inferred from rotation curve decompositions depend strongly on the adopted stellar mass-to-light ratios. Equal ($M_*/L_{K'}$) ratios for all galaxies on the one hand and a maximum-disk decomposition on the other hand lead to contradicting results when considering the luminous-to-dark mass ratios within the last measured points of the rotation curves.

- Decomposition fits with a Hernquist density profile for the dark matter halo give in general larger values of χ^2 than fits with an isothermal sphere density profile.

- There is a hint for a kinematic bimodality in the sense that, under the assumption of equal ($M_*/L_{K'}$)=0.6, the stellar disk rotation curves of high surface brightness galaxies peak above the rotation curves of the dark matter haloes near 2.2 scale lengths. In contrast, the rotational velocities of low surface brightness galaxies are dominated by the halo potential at the radii where the disk rotation curve reaches its maximum.

- Finally we have demonstrated for three galaxies of the same luminosity but with different surface brightnesses and compactness of the light distribution that their observed rotation curves can be decomposed using the same structural parameters for an isothermal dark halo and only minor differences in stellar mass-to-light ratios. For the two HSB examples, the potential of the luminous disk is dominant in the interior but for the LSB example, the halo is dominant at all radii.

Acknowledgements

This research has been supported by NATO Collaborative Research Grant 940271, Grants from the US National Science Foundation and the Leids Kerkhoven-Bosscha Fonds. The Westerbork Synthesis Radio Telescope used to obtain the rotation curves is operated by the Netherlands Foundation for Research in Astronomy (NFRA) with financial support from the Netherlands Organization for Scientific Research (NWO).

References

van Albada, T.S., and Sancisi, R., 1986, Phil. Trans. R. Soc. Lond. A, 320,447

Allen, C.W., 1973, *"Astrophysical Quantities"*, University of London, The Athlone Press

Begeman, K.G., 1987, PhD Thesis, University of Groningen

Begeman, K.G., 1989, A.&A., 223, 47

Begeman, K.G., Broeils, A.H. and Sanders, R.H., 1991, M.N.R.A.S., 249, 523

de Blok, W.J.G. and McGaugh, S.S., 1996, Ap.J., 469, 89

Bottema, R., 1993, A.&A., 275,16

Broeils, A.H., 1992, PhD Thesis, University of Groningen

Casertano, S. and van Gorkom, J.H., 1991, A.J., 101, 1231

Casertano, S. and van Albada, T.S., 1990, in *"Baryonic Dark Matter"*, Lynden-Bell, D. and Gilmore, G. (eds), Kluwer,Dordrecht, p.159

Casertano, S., 1983, M.N.R.A.S., 203, 735

Dalcanton, J.J., Spergel, D.N. and Summers, F.J., 1997, Ap.J., 482, 659

Dubinski, J. and Carlberg, R., 1991, Ap.J., 378, 496

Franx, M. and de Zeeuw, P.T., 1992, Ap.J., 392, L47

Freeman, K.C., 1970, Ap.J., 160, 811

Hernandez, X. and Gilmore, G., 1997, M.N.R.A.S., in press, astro-ph/9709167

Hernquist, L., 1990, Ap.J., 356, 359

Hoffman, Y., 1988, Ap.J., 328, 489

Kalnajs, A.J., 1983, in IAU Symp.100:*"Internal Kinematics of Galaxies"*, Athanassoula, A. (ed), Dordrecht, Reidel, p.87

Kent, S.M., 1986, A.J., 91, 1301

Kormendy, J., 1990, in *"The Edwin Hubble Centennial Symposium: The Evolution of the Universe of Galaxies"*. Kron, R.G. (ed), San Franciso, A.S.P., 33

van der Kruit, P.C. and Searle, L., 1981, A.&A., 95,105

Mathewson, D.S., Ford, V.L. and Buchhorn, M., 1992, Ap.J.Suppl., 81, 413

Milgrom, M., 1983, Ap.J., 270, 365

Navarro, J.F., Frenk, C.S. and White, S.D.M., 1997, Ap.J., submitted Nov.1996, astro-ph/9611107

Navarro, J.F., Frenk, C.S. and White, S.D.M., 1996, Ap.J., 462, 563

Olling, R.P., 1996, A.J., 112, 481

Persic, M., Salucci, P. and Stel, F., 1996, M.N.R.A.S., 281, 27

Persic, M. and Salucci, P., 1991, Ap.J., 368, 60

Rubin, V.C., Burstein, D., Ford Jr., W.K. and Thonnard, N., 1985, Ap.J. 289, 81

Sanders, R.H. and Begeman, K.G., 1994, M.N.R.A.S., 266, 360

Sicking, F.J., 1997, PhD Thesis, University of Groningen

Tully, R.B. and Verheijen, M.A.W., 1997, Ap.J., 484, 145

Tully, R.B., Verheijen, M.A.W., Pierce, M.J., Huang, J.-S. and Wainscoat, R.J., 1996, A.J., 112, 2471

Zaritsky, D., Smith, R., Frenk, C.S. and White, S.D.M, 1997, ApJ., 478, 53

Zwaan, M.A., van der Hulst, J.M., de Blok, W.J.G. and McGaugh, S.S., 1995, M.N.R.A.S., 273, 35

Appendix: The decompositions

This appendix contains a compilation of all the decompositions, presented in eight adjacent panels for each galaxy. The four left hand panels show the decompositions assuming an isothermal sphere model for the dark matter halo while a Hernquist density profile was assumed for the decompositions in the four right hand panels. The short dashed lines represent the rotation curves of the stellar component, the dotted lines show the contribution of the gaseous component and the long dashed lines indicate the rotational velocities induced by the potential of the spherical dark matter halo. The upper thick line shows the quadratic sum of the three components and is supposed to represent the observed rotation curve. The vertical arrows indicate $R_{25}^{b,i}$. The label in the upper left corner of each panel refers to the kind of fit that was made as explained in Section 5. The results of the fits are summarized in Tables 2a and 2b. The fits presented in panels N3992b1/c1, N4013b1, N4138b1 and U6923d2 resulted in extreme halo properties and should not be considered.

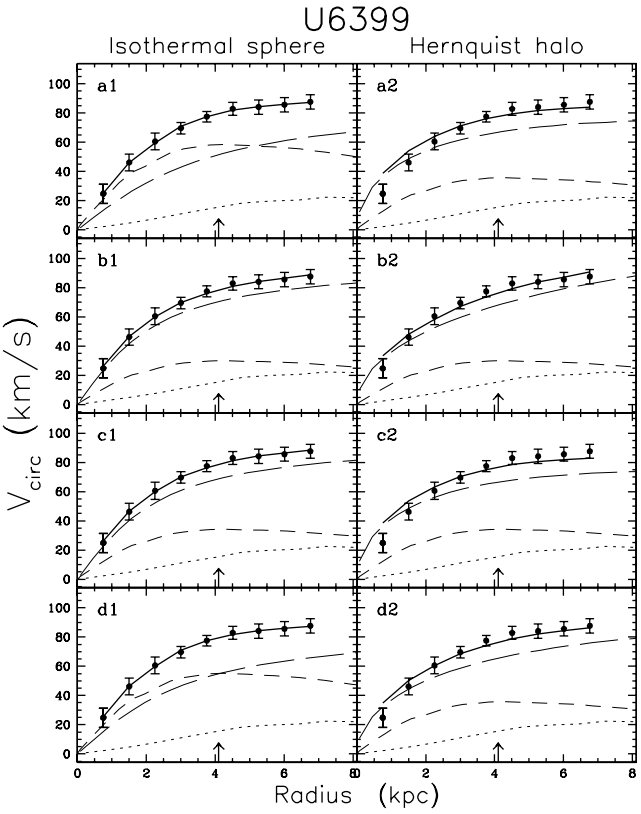

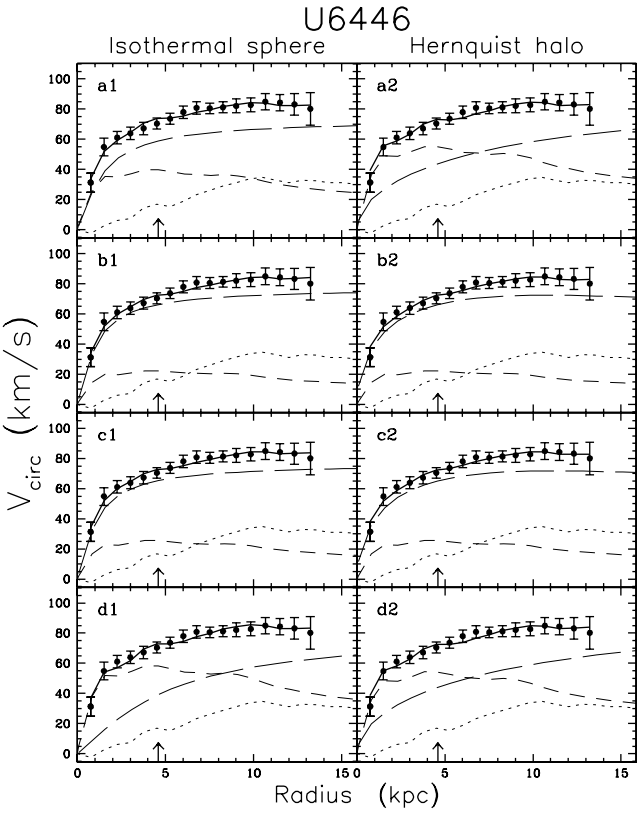

Tables 2a and 2b at the end of this appendix summarize the various mass-to-light ratios and structural parameters of the haloes.
Column (1) gives the NGC or UGC number.
Column (2) contains the stellar (M/L) ratio.
Column (3) gives the maximum rotational velocity of the rotation curve induced by the stars with the (M/L) ratio from the previous column.
Column (4) contains the maximum rotational velocity induced by the isothermal sphere.
Column (5) gives the halo core radius.
Column (6) provides the halo's central density.
Column (7) contains the weighted scatter of the observed point arround the fitted curve.
Columns (8-9) are similar to col.(2-3) except that these values relate to a Hernquist halo.
Column (10) gives the Hernquist halo mass.
Column (11) gives the truncation radius of the Hernquist halo.
Column (12) contains the global surface density calculated from M_0 and R_0.
Column (13) gives the maximum rotational velocity of the halo which occurs at the radius R_0.
Column (14) is similar to column (7) except that in this case a Hernquist model was fitted.

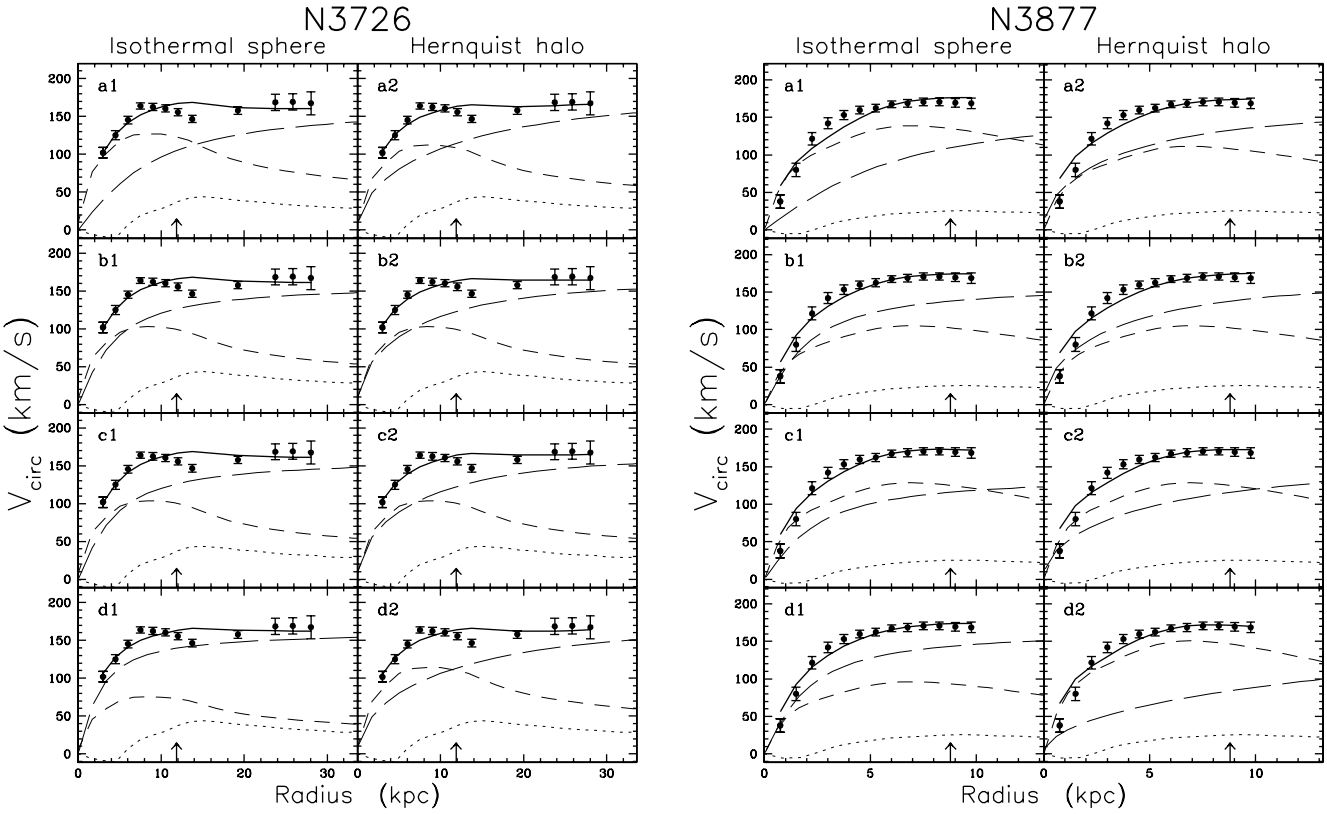
N3726
Isothermal sphere
Hernquist halo
a1
a2
b1
b2
c1
c2
d1
d2
V_{circ} (km/s)
Radius (kpc)

N3877
Isothermal sphere
Hernquist halo
a1
a2
b1
b2
c1
c2
d1
d2
V_{circ} (km/s)
Radius (kpc)

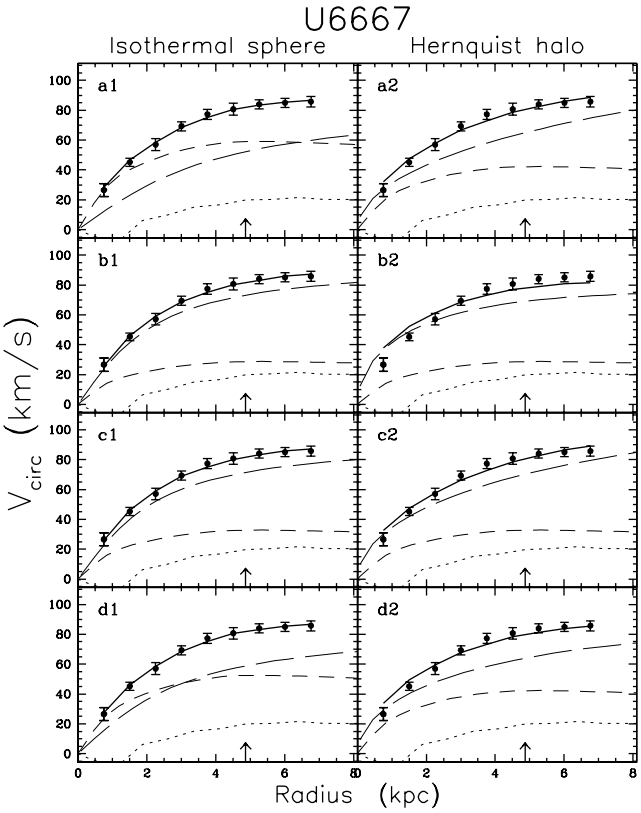
U6667
Isothermal sphere
Hernquist halo
a1
a2
b1
b2
c1
c2
d1
d2
V_{circ} (km/s)
Radius (kpc)

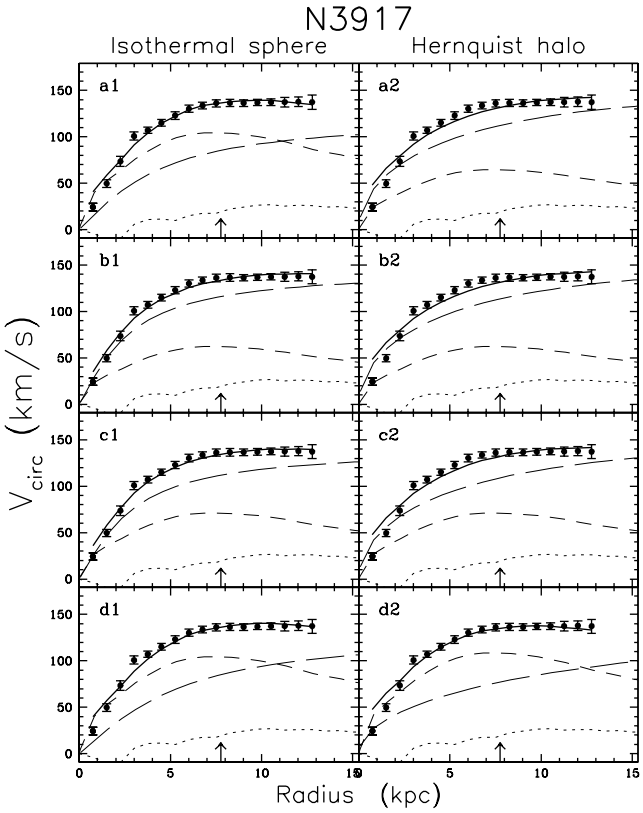
N3917
Isothermal sphere
Hernquist halo
a1
a2
b1
b2
c1
c2
d1
d2
V_{circ} (km/s)
Radius (kpc)

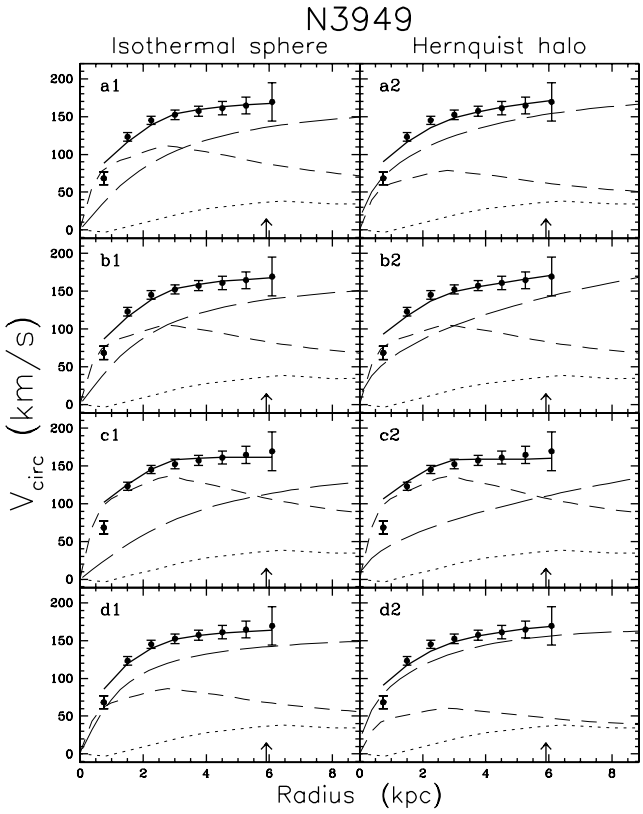
N3949
Isothermal sphere
Hernquist halo
a1
a2
b1
b2
c1
c2
d1
d2
V_{circ} (km/s)
Radius (kpc)

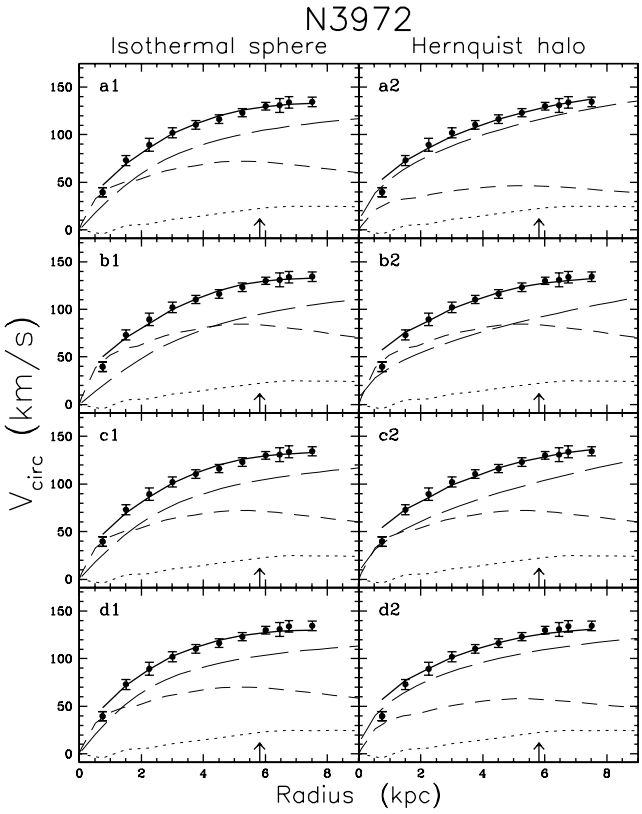
N3972
Isothermal sphere
Hernquist halo
a1
a2
b1
b2
c1
c2
d1
d2
V_{circ} (km/s)
Radius (kpc)

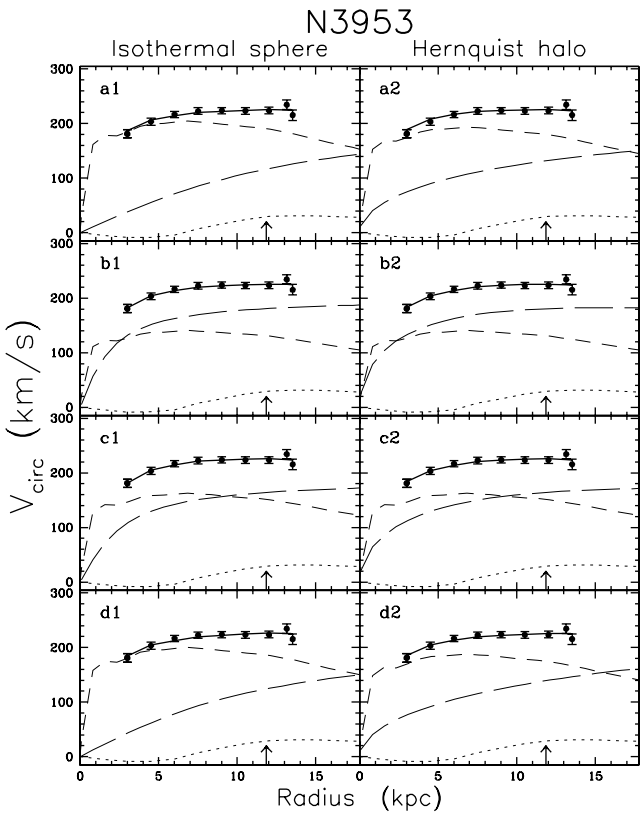
N3953
Isothermal sphere
Hernquist halo
a1
a2
b1
b2
c1
c2
d1
d2
V_{circ} (km/s)
Radius (kpc)

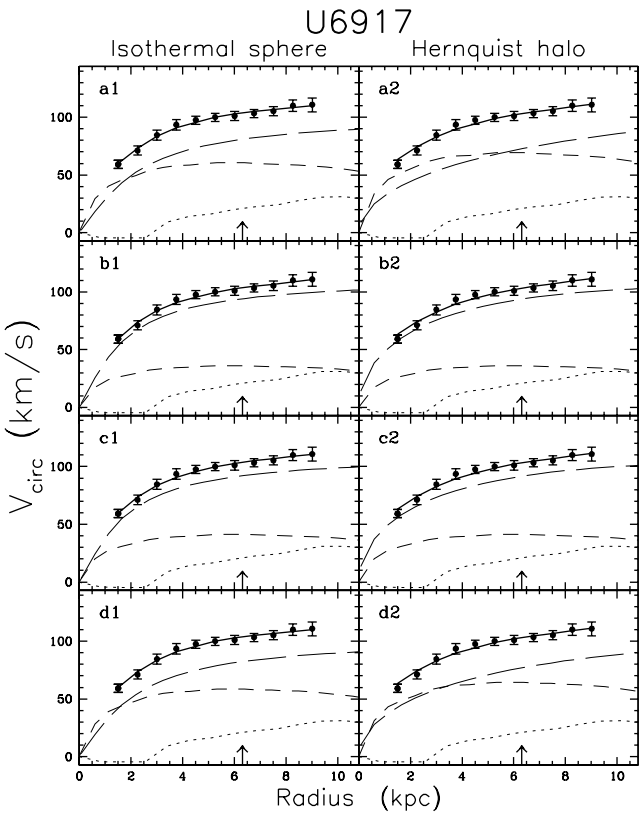
U6917
Isothermal sphere
Hernquist halo
a1
a2
b1
b2
c1
c2
d1
d2
V_{circ} (km/s)
Radius (kpc)

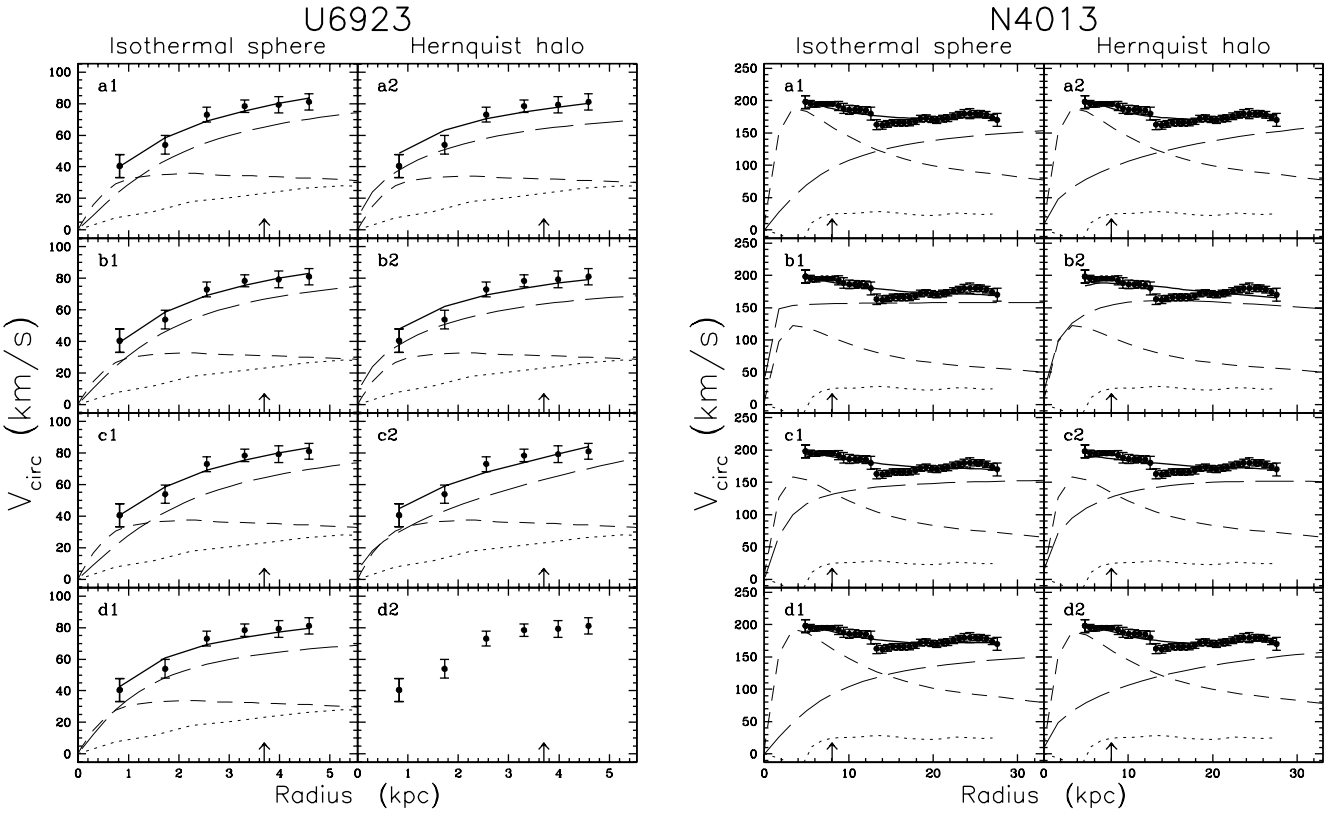
U6923
Isothermal sphere
Hernquist halo
N4013
Isothermal sphere
Hernquist halo
a1
a2
b1
b2
c1
c2
d1
d2
V_{circ} (km/s)
Radius (kpc)

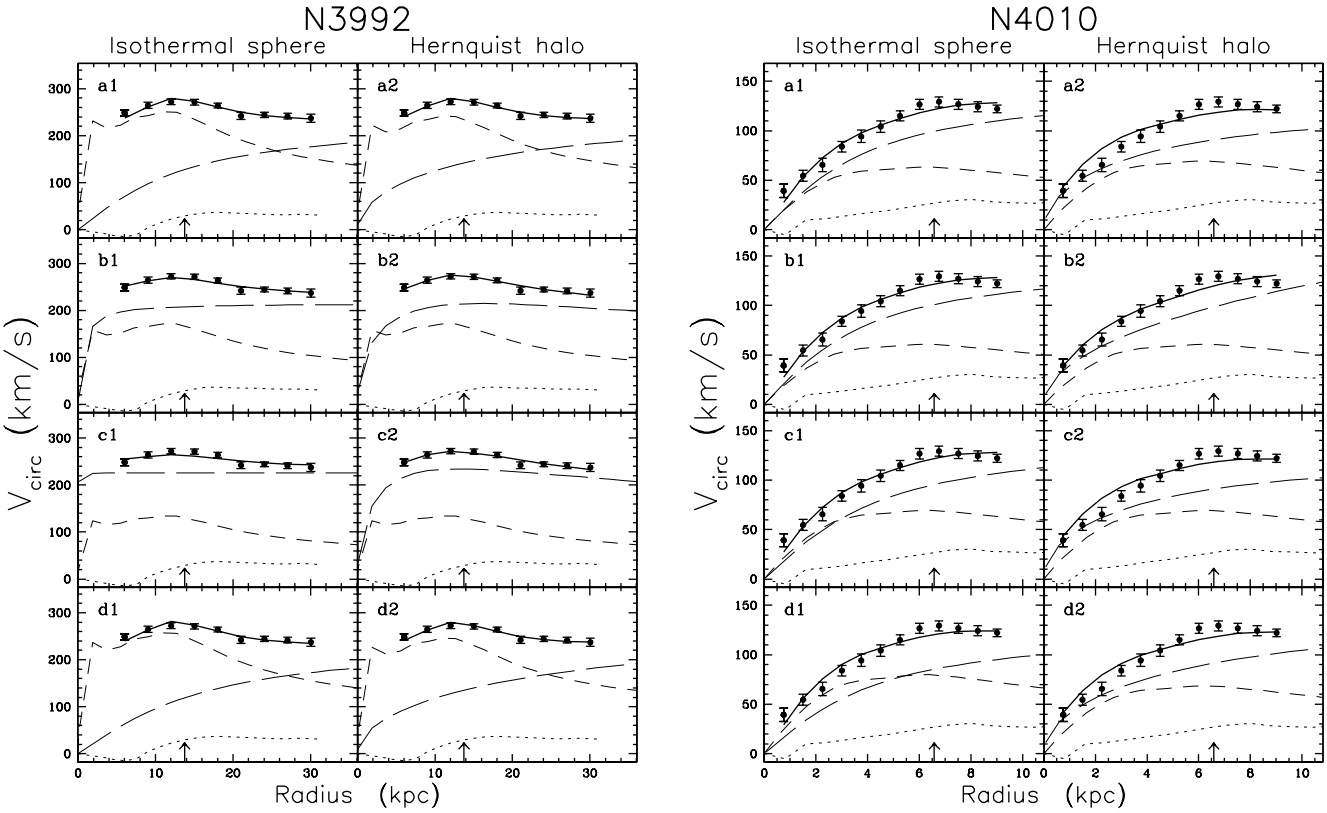
N3992
Isothermal sphere
Hernquist halo
N4010
Isothermal sphere
Hernquist halo
a1
a2
b1
b2
c1
c2
d1
d2
V_{circ} (km/s)
Radius (kpc)

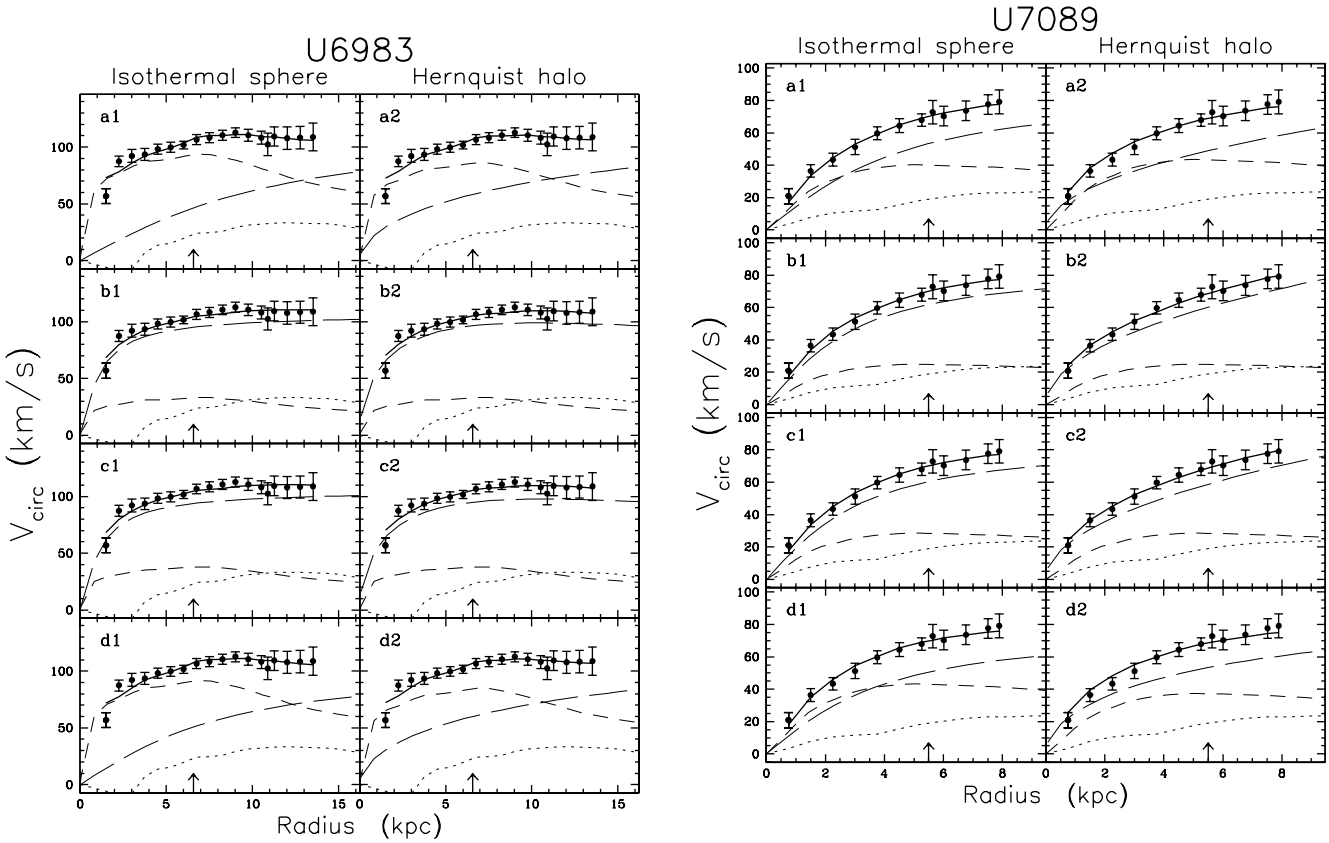
U6983
Isothermal sphere
Hernquist halo
a1
a2
b1
b2
c1
c2
d1
d2
V_{circ} (km/s)
Radius (kpc)

U7089
Isothermal sphere
Hernquist halo
a1
a2
b1
b2
c1
c2
d1
d2
V_{circ} (km/s)
Radius (kpc)

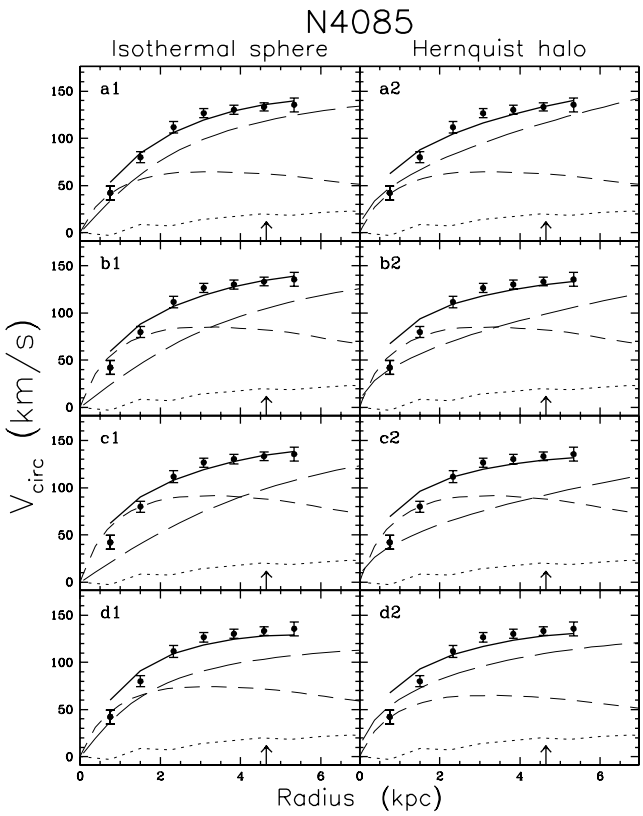
N4085
Isothermal sphere
Hernquist halo
a1
a2
b1
b2
c1
c2
d1
d2
V_{circ} (km/s)
Radius (kpc)

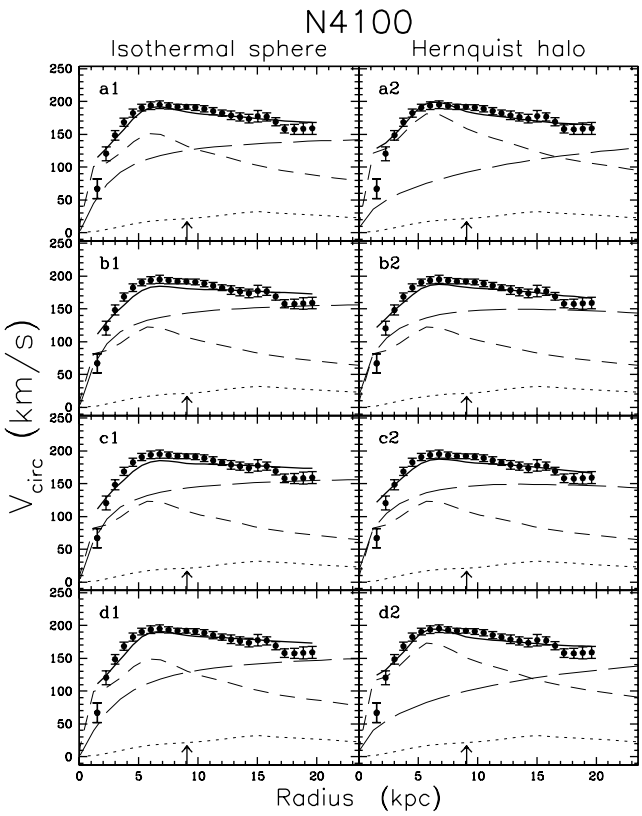
N4100
Isothermal sphere
Hernquist halo
a1
a2
b1
b2
c1
c2
d1
d2
V_{circ} (km/s)
Radius (kpc)

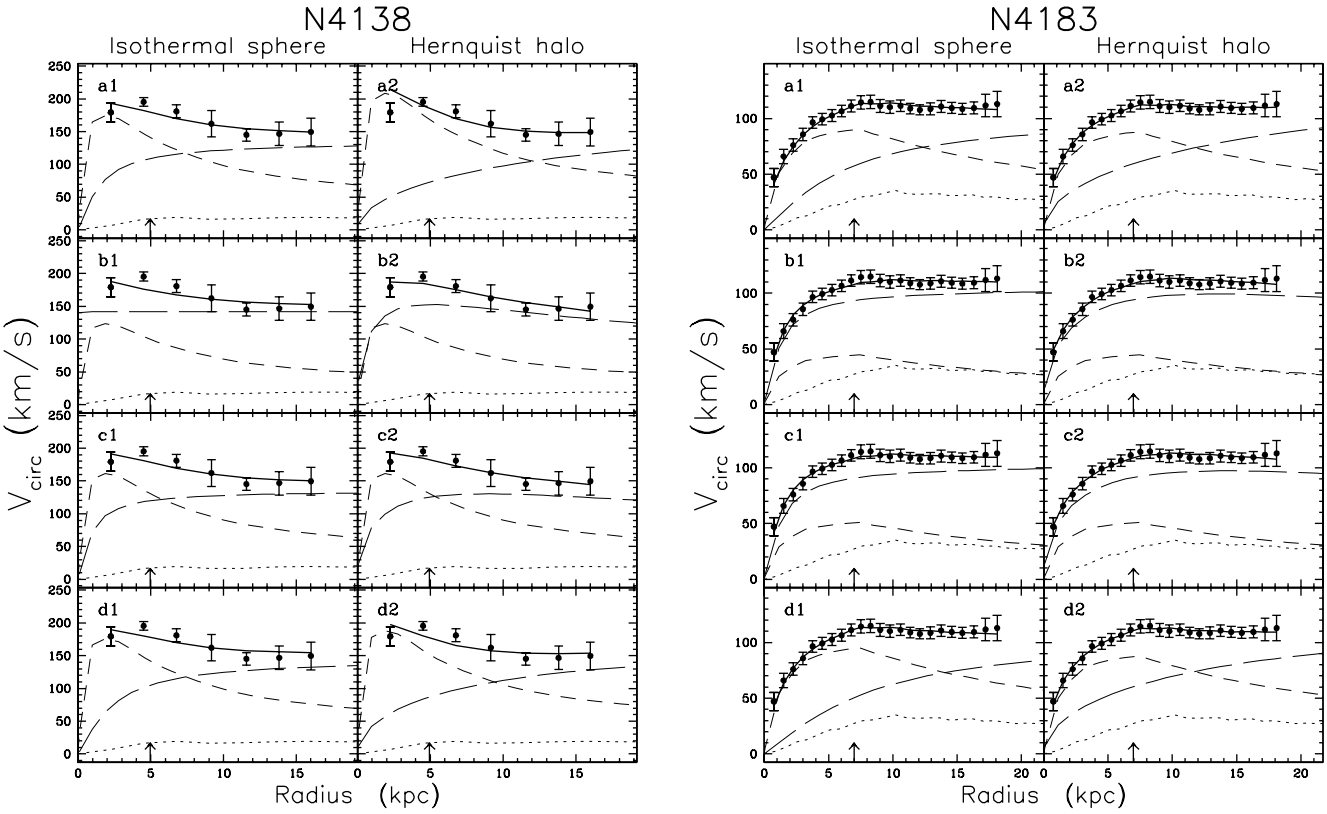
N4138
Isothermal sphere
Hernquist halo
N4183
Isothermal sphere
Hernquist halo
a1
a2
b1
b2
c1
c2
d1
d2
V_{circ} (km/s)
Radius (kpc)

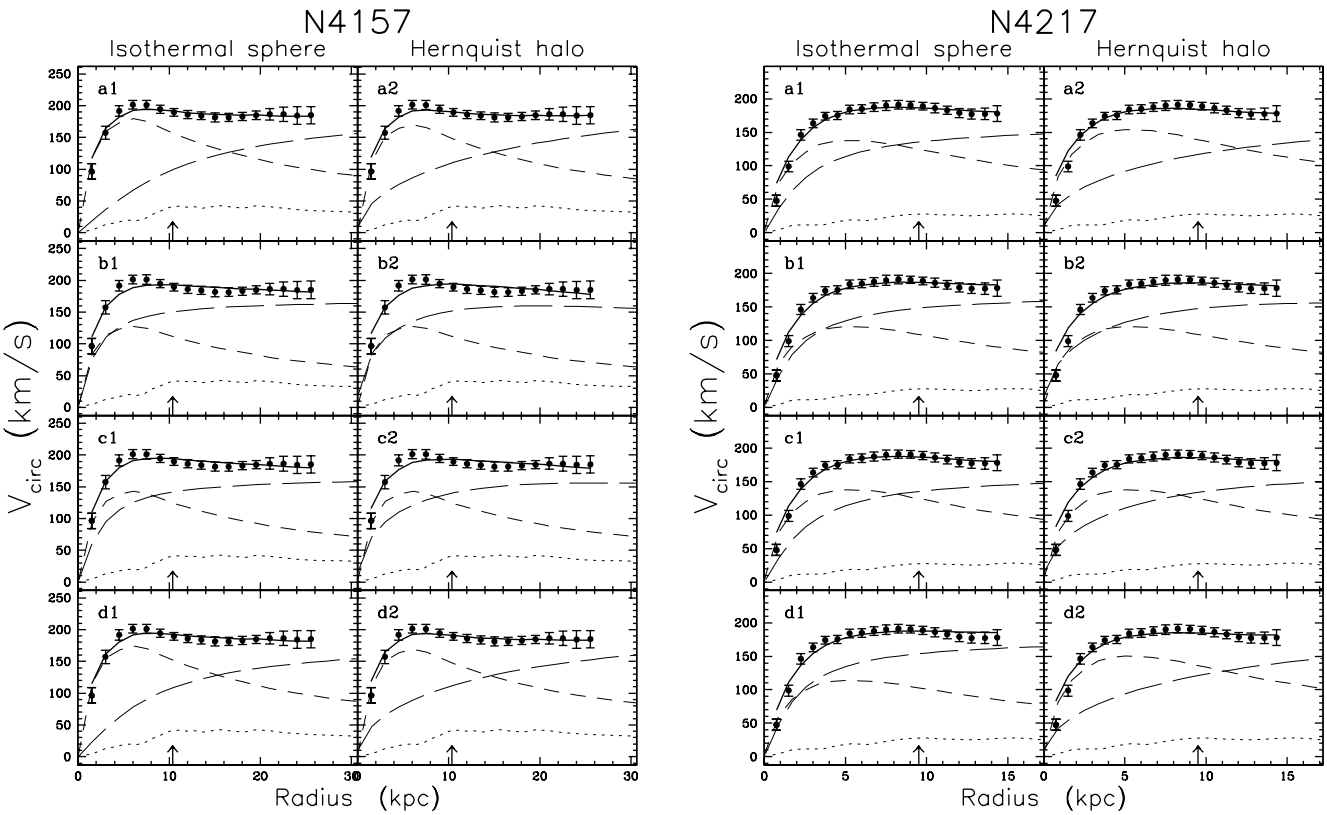
N4157
Isothermal sphere
Hernquist halo
N4217
Isothermal sphere
Hernquist halo
a1
a2
b1
b2
c1
c2
d1
d2
V_{circ} (km/s)
Radius (kpc)

Table 2a: Results from the rotation curve decompositions for an isothermal halo and a halo with a Hernquist density profile. The results in the upper part of this table were obtained by adopting the maximum-disk hypothesis. The lower part contains the results when assuming that the maximum rotational velocity of the HSB stellar disk is 63% of the observed maximum rotational velocity. Corresponding HSB-(M/L) values were averaged an uniformly applied to the LSB systems.

Name	Stellar disk		Isothermal halo				Stellar disk		Hernquist halo				
	$(\frac{M_*}{L_{K'}})$	V_{max}^{disk} (km/s)	V_∞ (km/s)	R_c (kpc)	ρ_0 ($M_\odot\,pc^{-3}$)	σ_w	$(\frac{M_*}{L_{K'}})$	V_{max}^{disk} (km/s)	M_0 ($10^{12}M_\odot$)	R_0 (kpc)	Σ_0 ($M_\odot\,pc^{-2}$)	V_{max}^{halo} (km/s)	σ_w (km/s)
(1)	(2)	(3)	(4)	(5)	(6)	(7)	(8)	(9)	(10)	(11)	(12)	(13)	(14)
Maximum-disk fits													
HSB galaxies													
N3726	0.90	127	169	7.1	0.010	10.0	0.70	112	2.06	78	54	169	10.0
N3877	0.70	139	171	4.8	0.023	9.1	0.45	111	0.53	25	136	151	8.8
N3949	0.40	111	180	2.1	0.141	7.5	0.20	78	0.51	18	262	176	8.7
N3953	0.95	205	228	10.1	0.009	4.1	0.85	193	2.10	67	75	184	4.4
N3972	0.60	72	144	2.4	0.069	3.1	0.25	47	1.34	44	110	181	4.4
N3992	2.10	251	235	10.6	0.009	5.2	1.95	242	4.00	95	71	214	4.4
N4013	0.85	188	179	6.4	0.015	5.8	0.85	188	3.34	103	50	187	5.1
N4085	0.30	65	172	2.1	0.121	5.4	0.30	65	295.80	654	110	699	8.7
N4100	0.90	151	153	2.2	0.090	7.6	1.30	182	2.28	94	41	162	7.7
N4138	0.70	174	135	1.3	0.193	11.1	1.00	208	1.81	80	45	156	12.0
N4157	0.95	179	199	9.3	0.009	5.5	0.85	170	4.39	117	51	201	5.6
N4217	0.60	138	164	2.2	0.099	6.7	0.75	154	1.15	49	75	159	8.9
LSB galaxies													
U6399	1.75	59	89	2.8	0.019	5.4	0.65	36	0.06	11	75	76	8.6
U6446	1.45	40	74	1.3	0.064	5.2	2.80	55	0.26	47	19	77	7.7
U6667	1.95	59	85	3.0	0.015	2.3	1.00	42	1.08	68	37	131	1.7
N3917	1.30	104	124	3.6	0.022	0.7	0.50	65	0.63	33	92	143	4.8
U6917	1.30	61	103	1.9	0.055	2.0	1.70	69	0.56	47	40	113	2.5
U6923	0.55	36	96	1.8	0.055	1.2	0.50	34	0.05	11	75	73	2.7
N4010	0.50	63	145	3.1	0.041	1.6	0.60	69	0.27	24	75	111	2.6
U6983	3.65	94	119	8.4	0.004	3.0	3.10	86	0.92	81	22	111	4.6
U7089	1.20	40	89	3.5	0.012	4.5	1.40	43	15.14	382	17	207	4.3
N4183	1.90	90	105	5.3	0.007	1.8	1.80	88	1.27	97	22	119	2.2
Bottema-disk fits													
HSB galaxies													
N3726	0.59	103	161	3.6	0.038	10.0	0.59	103	1.11	49	73	156	10.3
N3877	0.40	105	162	1.8	0.155	6.4	0.40	105	0.52	23	151	155	8.9
N3949	0.36	105	178	1.8	0.180	7.1	0.36	105	6.89	87	144	292	8.9
N3953	0.45	141	201	1.6	0.302	3.6	0.45	141	0.50	16	308	183	3.6
N3972	0.82	84	147	3.2	0.040	3.9	0.82	84	24.37	264	56	316	5.6
N3992	0.98	172	215	0.6	2.314	4.1	0.98	172	0.69	16	422	215	3.7
N4013	0.36	123	...	...	...	6.5	0.36	123	0.35	15	265	161	8.9
N4085	0.52	85	184	3.3	0.059	7.0	0.52	85	107.82	464	80	501	10.0
N4100	0.59	122	165	1.5	0.212	10.4	0.59	122	0.28	14	244	150	8.6
N4138	0.35	123	...	...	...	14.5	0.35	123	0.11	5	677	153	8.7
N4157	0.48	128	171	1.7	0.197	6.8	0.48	128	0.47	20	192	160	8.0
N4217	0.46	121	171	1.7	0.181	6.9	0.46	121	0.43	19	190	157	9.3
LSB galaxies													
U6399	0.46	30	99	1.7	0.062	4.7	0.46	30	0.58	43	50	121	8.7
U6446	0.46	23	78	0.9	0.135	5.5	0.46	22	0.05	11	72	73	6.4
U6667	0.46	29	96	1.7	0.062	2.6	0.46	29	0.06	11	75	75	2.5
N3917	0.46	62	147	2.3	0.078	1.1	0.46	62	0.61	32	95	144	3.4
U6917	0.46	36	113	1.5	0.117	1.8	0.46	36	0.17	17	98	105	2.0
U6923	0.46	33	95	1.6	0.065	1.3	0.46	33	0.05	10	75	72	5.4
N4010	0.46	61	145	3.0	0.044	1.6	0.46	61	15.36	205	58	284	2.5
U6983	0.46	33	107	1.0	0.223	2.9	0.46	33	0.09	10	140	99	4.7
U7089	0.46	25	88	2.4	0.025	3.8	0.46	25	8.93	236	26	202	3.8
N4183	0.46	45	105	1.0	0.185	1.8	0.46	45	0.12	13	109	100	1.8

Table 2b: Results from the rotation curve decompositions for an isothermal halo and a halo with a Hernquist density profile. The results in the upper part of this table were obtained by assuming that all galaxies have the same stellar mass-to-light ratio in the K'–band of 0.6 which is the maximum value allowed without severly violating the maximum observed rotational velocity in any galaxy. Results in the lower part of this table were obtained by contraining one of the halo parameters.

Name	Stellar disk		Isothermal halo				Stellar disk		Hernquist halo				
	$(\frac{M_*}{L_{K'}})$	V_{max}^{disk} (km/s)	V_∞ (km/s)	R_c (kpc)	ρ_0 ($M_\odot\,pc^{-3}$)	σ_w	$(\frac{M_*}{L_{K'}})$	V_{max}^{disk} (km/s)	M_0 ($10^{12}M_\odot$)	R_0 (kpc)	Σ_0 ($M_\odot\,pc^{-2}$)	V_{max}^{halo} (km/s)	σ_w (km/s)
(1)	(2)	(3)	(4)	(5)	(6)	(7)	(8)	(9)	(10)	(11)	(12)	(13)	(14)
Equal-($M_*/L_{K'}$) fits													
HSB galaxies													
N3726	0.60	104	161	3.6	0.037	10.0	0.60	104	1.15	51	71	156	10.3
N3877	0.60	129	139	2.0	0.088	6.6	0.60	129	0.61	33	91	142	8.4
N3949	0.60	136	169	3.0	0.059	10.4	0.60	136	364.39	869	77	673	12.1
N3953	0.60	163	189	2.1	0.149	3.5	0.60	163	0.61	22	199	173	3.6
N3972	0.60	72	144	2.4	0.069	3.1	0.60	72	47.28	330	69	393	4.8
N3992	0.60	134	...	...	...	6.9	0.60	134	0.67	13	621	235	3.7
N4013	0.60	158	161	2.0	0.116	6.4	0.60	158	0.59	27	124	152	7.4
N4085	0.60	92	197	4.1	0.043	7.8	0.60	92	187.99	659	69	555	10.8
N4100	0.60	123	165	1.6	0.204	10.3	0.60	123	0.26	14	240	149	8.5
N4138	0.60	161	136	0.8	0.554	11.7	0.60	161	0.14	9	288	131	9.6
N4157	0.60	143	167	2.2	0.111	6.2	0.60	143	0.61	27	135	156	7.4
N4217	0.60	138	164	2.2	0.099	6.7	0.60	138	0.63	29	124	155	8.9
LSB galaxies													
U6399	0.60	34	97	1.8	0.057	4.7	0.60	34	0.06	11	75	75	8.4
U6446	0.60	26	77	0.9	0.123	5.4	0.60	26	0.05	11	68	72	7.7
U6667	0.60	33	95	1.7	0.057	2.4	0.60	33	0.54	43	46	116	2.4
N3917	0.60	71	143	2.4	0.067	1.0	0.60	71	0.67	36	84	143	5.0
U6917	0.60	41	112	1.5	0.101	1.9	0.60	41	0.18	18	91	104	2.0
U6923	0.60	37	97	1.9	0.049	1.2	0.60	37	26.89	324	41	299	2.9
N4010	0.60	69	146	3.5	0.033	1.6	0.60	69	0.27	24	75	111	2.5
U6983	0.60	38	106	1.0	0.205	3.1	0.60	38	0.09	11	133	98	4.1
U7089	0.60	28	87	2.5	0.022	3.8	0.60	28	34.60	482	24	278	3.8
N4183	0.60	51	103	1.1	0.158	1.8	0.60	51	0.13	14	99	98	1.7
Constrained-halo fits													
HSB galaxies													
N3726	0.32	75	162	2.2	0.101	9.7	0.73	114	1.73	71	55	162	9.6
N3877	0.33	96	167	1.7	0.185	6.3	0.82	151	3.09	120	34	167	7.9
N3949	0.24	86	164	1.1	0.437	6.2	0.12	60	0.28	11	354	164	8.5
N3953	0.91	200	223	8.7	0.012	3.9	0.80	188	4.43	96	76	223	3.9
N3972	0.57	70	134	1.9	0.092	3.6	0.38	58	0.37	22	119	134	5.9
N3992	2.20	257	242	12.5	0.007	5.1	2.02	246	7.99	147	59	242	4.4
N4013	0.89	193	177	6.6	0.013	5.5	0.86	189	2.57	89	52	177	5.1
N4085	0.40	74	134	1.5	0.156	8.5	0.30	65	0.29	17	154	134	10.6
N4100	0.88	149	164	2.7	0.067	8.4	1.18	173	1.94	78	51	164	8.2
N4138	0.71	175	147	2.1	0.096	12.6	0.81	188	0.92	46	69	147	13.6
N4157	0.89	174	185	6.9	0.013	5.8	0.84	169	2.89	91	55	185	5.6
N4217	0.41	114	178	1.7	0.197	7.2	0.71	150	1.81	62	76	178	8.8
LSB galaxies													
U6399	1.56	55	88	2.4	0.027	5.6	0.65	36	0.15	21	56	88	7.2
U6446	3.12	58	82	4.4	0.006	5.6	2.71	54	0.34	54	18	82	6.9
U6667	1.54	53	86	2.3	0.026	1.8	1.00	42	0.17	24	45	86	1.7
N3917	1.30	104	135	4.5	0.017	0.7	1.41	109	1.32	78	34	135	3.5
U6917	1.22	59	104	1.8	0.006	2.5	1.47	64	0.32	32	50	104	2.5
U6923	0.49	34	81	1.1	0.096	1.1	...	..	...	..	...	..	3.2
N4010	0.79	80	128	3.3	0.028	1.6	0.58	69	0.56	37	65	128	2.5
U6983	3.49	92	107	6.4	0.005	3.9	3.00	85	0.74	69	24	107	
U7089	1.38	43	79	3.0	0.012	4.5	1.03	37	0.21	36	25	79	4.3
N4183	2.10	95	109	7.0	0.005	2.0	1.79	88	0.84	76	23	109	3.0